國 立 交 通 大 學
光 電 工 程 研 究 所

碩士論文

40GHz 主動諧波鎖模光纖雷射之研究

Study of 40GHz Active Harmonic Mode-locked Erbium-doped Fiber Lasers

研 究 生：蔡馥宇

指導老師：祁　甦 博士

陳智弘 博士

中 華 民 國 九 十 三 年 六 月

40GHz 主動諧波鎖模光纖雷射之研究

Study of 40GHz Active Harmonic Mode-locked Erbium-doped Fiber Lasers

研 究 生：蔡馥宇　　Master：Fu-Yu Tsai

指導老師：祁　甦 博士　　Advisor：Dr. Sien Chi

陳智弘 博士　　Dr. Jye-Hong Chen

國 立 交 通 大 學

光 電 工 程 研 究 所

碩 士 論 文

A Thesis

Submitted to Institute of Electro-Optical Engineering

College of Electrical Engineering and Computer Science

National Chiao Tung University

In Partial Fulfillment of the Requirements

For the Degree of

Master

In

Institute of Electro-Optical Engineering

June 2003 Hsinchu, Taiwan, Republic of China

中 華 民 國 九 十 三 年 六 月

40GHz 主 動 諧 波 鎖 模 光 纖 雷 射 之 研 究

研究生：蔡馥宇　　指導老師：祁　甦 博士

陳智弘 博士

國立交通大學光電工程研究所碩士班

摘要

近幾年來，光纖通訊系統對於高傳輸速率與高傳輸量的需求日漸龐大，因此一個穩定而且擁有短脈衝、高脈衝重複率、高超模抑制率、高能量輸出脈衝序列的光源在這之中扮演了一個關鍵性的角色，而主動諧波鎖模雷射就是一個絕佳的選擇。

在論文中，我們順利的架設了一個 40GHz 的主動諧波鎖模光纖雷射，此雷射的共振腔全都是由偏振態維持光纖所組成；當雷射操作在脈衝重複率為 20GHz 及 40GHz 時，所獲得的脈衝寬度分別為 7.81ps 以及 3.31ps，平均功率約為 1mW，超模抑制率可超過 50dB 以上；在模擬的部分，模擬的結果非常接近我們的實驗結果，這也證實了 VPI 可成功的模擬主動鎖模光纖雷射。

Study of 40GHz Active Harmonic Mode-locked Erbium-doped Fiber Lasers

Master：Fu-Yu Tsai Advisor: Dr. Sien Chi

Dr. Jye-Hong Chen

Institute of Electro-optical Engineering
College of Electrical Engineering and Computer Science
National Chiao-Tung University

Abstract

The demand for the ultrahigh-speed and ultralarge-capacity optical fiber transmission systems is becoming larger and larger in recent years. Therefore, a stable optical short pulse source with high repletion rate, high SMSR, and high output power pulse train plays as an important role. As mentioned above, they can be achieved by active harmonic mode-locked erbium-doped fiber lasers.

In this study, a 40GHz active harmonic mode-locked erbium-doped fiber laser is demonstrated. The fiber cavity consists of all polarization maintain fiber. The pulsewidth 7.81ps and 3.31ps respectively operated at 20GHz and 40GHz was obtained. The average output power is about 1mW and the super-mode suppression ratio (SMSR) is above 50dB. In the simulation section, the simulation results are all close to the experimental results. Active mode-locked fiber ring lasers can be successfully simulated by using VPI.

誌　　謝

Acknowledgements

雖然這不是一部完美的論文，但這部論文的完成，要感謝的人真的很多，僅以此文表達我的誠摯謝意。

首先，感謝我的指導老師祁甦老師與陳智弘老師，引領我進入光纖通訊的領域，因為有他們專業的指導，讓我不論是在求學或研究的過程中獲益良多；同時，除了課業方面，老師們也使我學習到許多寶貴待人處事的道理，是我學習效法的對象。感謝賴暎杰老師的指導，讓我在實驗上的困惑得到了改進與解釋。

研究的過程中，幸賴許多師長朋友的協助，讓我得以度過挫折與困難。論文能順利付梓，感謝項維巍學長、彭朋群學長在實驗的理論與架構方面，提供了許多經驗分享，謝謝彭煒仁學長、黃明芳學姊以及已經畢業的葉信宏學長在實驗的設備與量測方面，常常從旁協助讓我得以順利完成實驗。特別是項維巍學長，他總是不厭其煩的回答我很多問題，讓我見識到深厚的理論基礎與實驗經驗。

要感謝的人，當然還有實驗室的好伙伴嘉建與盈傑，在與他們討論的過程中，常常讓我獲益匪淺。謝謝宥燁陪我一起討論模擬。還有謝謝偉志、峰生與建宏的熱情相助，讓我的實驗進行順利。感謝加和、至揚、淑玲與學弟們昱璋、炫涵、崇佑陪我度過那一段整日泡在儀器堆裡的日子，有你們的陪伴生活增添不少繽紛色彩。同時也要感謝賴老師實驗室的宗正與坤璋，在實驗與儀器上幫了不少忙。此外，更有賴許多朋友的精神支持，挂一漏萬，要感謝的人太多了，可能尚有一些未提及的朋友們，在此均一併致謝。

最後將這篇論文獻給總是在背後默默支持我的父母，謝謝你們對我的付出與栽培，僅以此篇論文與你們獻上我最高的謝意。

2004.6.9 于風城交大

Contents

Acknowledgements

Chinese abstract

English abstract

Contents

List of Figures

List of Tables

CHAPTER 1 Introduction

1.1 The history of fiber lasers……1

1.2 The motivation of research……..5

1.3 The structure of the thesis……7

CHAPTER 2 The Theory of Mode-Locked Laser

2.1 Theory of mode-locked lasers…….…..8

2.2 Active mode-locked lasers……...14

2.2.1 Amplitude modulation mode-locking……..14

2.2.2 Phase modulation mode-locking…….16

2.2.3 Harmonic mode-locking……..18

2.2.4 Rational harmonic mode-locking……20

2.3 Stabilization of mode-locked lasers……..……..21

2.3.1 Regenerative mode-locking…….21

2.3.2 Phase-locked loop (PLL)…….23

CHAPTER 3 Experimental Setup and Results

3.1 Introduction of the experiment……25

3.2 Setup of the experiment (Operating at 2GHz and 10GHz)…….29

3.2.1 Operating at 2GHz……..30

3.2.2 Operating at 10GHz……35

3.3 Setup of the experiment (Operating at 10GHz, 20GHz and 40GHz)……..38

3.3.1 Operating at 10GHz……39

3.3.2 Operating at 20GHz……42

3.3.3 Operating at 40GHz……45

CHAPTER 4 Simulations

4.1 Introduction of VPI……48

4.2 Simulations……52

4.3 Experimental simulation……56

4.3.1 Simulation results of 2GHz……58

4.3.2 Simulation results of 10GHz……...59

4.3.3 Simulation results of 20GHz……...62

4.3.4 Simulation results of 40GHz……...63

CHAPTER 5 Conclusions & Discussions

5.1 Summary of achieved results……..66

5.2 Future research and Improvement…...……67

References……..70

List of Figures

Figure 2.1 initial state of optical field in laser cavity

Figure 2.2 (a) the electric field of individual frequency $\omega_q, \omega_{q+1}, \omega_{q+2}$ and they have fixed relation of the phase. (b) total electric field (c) total optical field.

Figure 2.3 the distribution of electric field (left hand side) of once (a), two (b), three round trip times (c) of the cavity and its optical spectrum (right hand side)

Figure 2.4 Illustration of the mode-locked pulse train as M=4

Figure 2.5 Principle of active mode-locking explained in the time domain [24]

Figure 2.6 Principle of actively mode-locking explained in the frequency domain

Figure 2.7 Time domain of phase modulation

Figure 2.8 Development of pulse train in time domain by superposition of modes

Figure 2.9 Experimental setup for the harmonically and regeneneratively mode-locked erbium-doped fiber laser [30].

Figure 2.10 Mode-locked Erbium-doped fiber ring laser and stabilization scheme (Dashed line), where “PC” is polarization controller and “SID” is step index fiber [7]

Figure 3.1 The experimental setup, where “PC” is polarization controller.

Figure 3.2 **(a**) Operating current versus output power of the pumping laser **(b)** Optical spectrum of pumping laser diode operated at 200mA

Figure 3.3 Gain profile of PM-EDF pumped by different pumping power

Figure 3.4 3dB bandwidth of optical tunable filter (center wavelength at 1550nm)

Figure 3.5 The experimental setup with 10GHz JDSU amplitude modulator

Figure 3.6 **(a)** output of laser operated at 2GHz without polarization controller. **(b)** output of laser operated at 10GHz without polarization controller.

Figure 3.7 The waveform operated at 2GHz is measured by Agilent 86105A in different time window spans.

Figure 3.8 Optical spectrum

Figure 3.9 RF spectrum **(a)** span: 20MHz, SMSR: 58dB **(b)** span: 500MHz, SMSR: 55 dB

Figure 3.10 The pulsewidth is changed by using the polarization controller. Pulsewidth **(a)** 82 ps **(b)** 66ps **(c)** 56ps **(d)** 39ps.

Figure 3.11 The waveform operated at 10GHz is measured by Agilent 86116A in different time window spans.

Figure 3.12 Optical spectrum

Figure 3.13 The waveform measured by autocorrelator (The solid line is Gaussian fitting curve)

Figure 3.14 RF spectrum **(a)** span: 20MHz, SMSR: 52dB **(b)** span: 100MHz, SMSR: 53dB

Figure 3.15 The experimental setup

Figure 3.16 The waveform operated at 10GHz is measured by Agilent 86116A in different time window spans.

Figure 3.17 Optical spectrum

Figure 3.18 The waveform measured by autocorrelator (The solid line is Gaussian fitting curve)

Figure 3.19 RF spectrum, span: 100MHz, SMSR: 53 dB

Figure 3.20 The waveform operated at 20GHz is measured by Agilent 86116A in different time window spans.

Figure 3.21 The 20GHz pulse train measured by autocorrelator (The solid line is

Gaussian fitting curve)

Figure 3.22 The waveform measured by autocorrelator (The solid line is Gaussian fitting curve)

Figure 3.23 Optical spectrum

Figure 3.24 RF spectrum, span: 50MHz, SMSR: 56 dB

Figure 3.25 The waveform operated at 40GHzHz is measured by Agilent 86116A in different time window spans.

Figure 3.26 The 40GHz pulse train measured by autocorrelator

Figure 3.27 The waveform measured by autocorrelator (The solid line is Gaussian fitting curve)

Figure 3.28 Because of some perturbations, the phase between the modes is not locked and eventually instability occurs.

Figure 3.29 Optical spectrum

Figure 4.1 Bidirectional simulation algorithm. Step1 and 2 are repeated to build up a waveform [31].

Figure 4.2 Passing data unidirectionally simplifies calculations and slows data to be processed efficiently in blocks [31].

Figure 4.3 Considerations when developing a model [31]

Figure 4.4 The experiment structure [30].

Figure 4.5 (a) optical spectrum (b) Changes in pulsewidth and output power against pumping power [30]

Figure 4.6 Waveform of simulating output pulse train without dispersion shift fiber (Full Width Half Maximum (FWHM): 7.15ps)

Figure 4.7 Waveform of simulating output pulse train with dispersion shift fiber (FWHM: 3.02ps)

Figure 4.8 Optical spectrum of 3.02ps pulsewidth

Figure 4.9 The simulation structure of VPI

Figure 4.10 Waveform of AML-EFRL operated at 2GHz. (FWHM: 47.03ps)

Figure 4.11 Optical spectrum; the simulation result is shown in the left figure and the right one is the experimental result.

Figure 4.12 Waveform of AML-EFRL operated at 10GHz. (FWHM: 20.55ps)

Figure 4.13 Optical spectrum; the simulation result is shown in the left figure and the right one is the experimental result.

Figure 4.14 Waveform of AML-EFRL operated at 10GHz without OTF. (FWHM: 10.02ps)

Figure 4.15 Optical spectrum without OTF; the simulation result is shown in the left figure and the right one is the experimental result.

Figure 4.16 Waveform of AML-EFRL operated at 20GHz without OTF. (FWHM: 7.75ps)

Figure 4.17 Optical spectrum without OTF; the simulation result is shown in the left figure and the right one is the experimental result.

Figure 4.18 Waveform of AML-EFRL operated at 40GHz without OTF. (FWHM: 4.40 ps)

Figure 4.19 Optical Spectrum without OTF; the simulation result is shown in the left figure and the right one is the experimental result.

Figure 5.1 AML-EDFL and stabilizing scheme (dashed line); where “DBM” is double balance mixer and “LP filter” is low pass circuit.

List of Tables

Table 3.1 The specification of devices used in the fiber ring cavity

Table 3.2 Parameters of the mode-locked laser operated at 2GHz repetition rate

Table 3.3 Parameters of the mode-locked laser operated at 10GHz repetition rate

Table 3.4 Parameters of the mode-locked laser operated at 10GHz repetition rate

Table 3.5 Parameters of the mode-locked laser operated at 20GHz repetition rate

Table 3.6 Parameters of the mode-locked laser operated at 40GHz repetition rate

Table 4.1 Comparison between simulation and experimental result.

Table 4.2 **(a)** The detailed characteristic of components using in VPI simulation [32]

Table 4.2 **(b)** The detailed characteristic of components using in VPI simulation [32]

Table 4.3 Comparing the results of simulation with that of experiment.

Table 4.4 Comparing the results of simulation with that of experiment.

Table 4.5 Comparing the results of simulation with that of experiment.

Table 4.6 Comparing the results of simulation with that of experiment.

Table 4.7 Comparing the results of simulation with that of experiment.

CHAPTER 1

Introduction

1.1 The history of fiber lasers

In early 1930, there have been some scientists purposed to use fiber as a medium of transmission waveguide of the light. However, in that age, the manufacture of purification of glass and technology of semiconductor was not developed as well as what we see today. Besides, there was no reliable light source, and the insertion loss of fiber was very large. The loss of transmission was above 1000dB per kilometer before. Therefore, it didn't not adapt to fiber optical communication system. Until 1960, Maiman, an America scientist, demonstrated a ruby laser and the first laser was born in the world. In 1962, Hall and Nathan etc la, they invented a GaAs semiconductor laser. It improved the idea of transmission of using fiber as a medium of the waveguide. In 1966, Gao-kun, a scientist of non-Chinese citizen of Chinese origin, proposed this idea. The great contributions of these people open the door of the studies of the fiber optical communication system.

A fiber amplifier can be converted into a laser by placing it inside a cavity designed to provide optical feedback. Such lasers are called fiber lasers. Many kinds of rare-earth ions, such as erbium (Er), neodymium (Nd), and ytterbium (Yb), can be used to make fiber lasers capable of operating over a wide range of wavelength extending from 0.4 to 4μm. The first fiber laser, demonstrated in 1961, was based on an Nd-doped fiber with 300μm core diameter, but it had high insertion loss [1]. In 1973, low-loss silica fibers were used to build diode-pumped fiber lasers and soon after such fibers became available [2].

However, it was not until the late 1980s that fiber lasers began to attract a lot of interests in research. The initial main emphases of the research were on Nd- and Er-doped fiber lasers. Nd-doped fiber lasers are of considerable practical interest since they can be pumped by GaAs semiconductor lasers operating near $0.8\,\mu m$. On the other hand, Er-doped fiber lasers can operate in several wavelength regions, ranging from visible to far infrared. The wavelength of $1.55\,\mu m$ regions has attracted the most attention because it coincides with the low-loss region of silica fibers for optical communication applications.

The performance of Erbium-doped fiber lasers (EDFLs) improves considerably while they are pumped at the 980 or 1480nm wavelength, because of the absence of the excited-state absorption. The 980nm pump wavelength yields higher gains than a 1480nm pump at high powers. This comes from the fact that 980nm has achieved a higher inversion than 1480nm. But the amplified spontaneous emission (ASE) starts growing as the pump power is increased; the higher inversion created at the beginning of the fiber by the 980 pump creates a better seed for the forward ASE than that created by the 1480nm pump [3]. In public, there are three kinds of pumping mechanism: forward pumping, backward pumping, and bidirectional pumping. Furthermore the wavelength of pumping power and pumping mechanisms are decided by the applications and demands of the EDFLs.

As early as 1989, a 980nm-pumped EDFL exhibited a slope efficiency of 58% against the absorbed pump power [4]. They also exhibited good performances when pumped at 1480nm. The choices between the pumping wavelength 980 and 1480nm and structures are not always clear since each pumping way has its own merits.

In a 1989 experiment on active mode-locking, 4ps pulses were generated by using a ring cavity which included 2km of standard fibers with large anomalous GVD [5]. In 1992, a fiber laser provided 3.5 to 10ps pulses with a transform-limited time-bandwidth product of 0.32 at the repetition rate up to 20GHz [6]. The laser was used in a system experiment to demonstrate such a laser source which can be used in soliton communication systems at the bit rate up to 8Gb/s. In the same year, a stabilization scheme for a mode-locked erbium fiber laser which relies on locking the pulse phase with that of the drive source was reported [7]. In 1993, a EDFL produced 6ps pulses at the repetition rate up to 40GHz and with the output wavelength tunable over a wide range of 40 to 50nm [8]. In 1999, the technique of regenerative mode locking with phase-locked loop (PLL) produced a 40GHz pulse train with tuning range from 1530 to 1560nm and pulsewidth as short as 0.9ps by using a soliton effect in the fiber cavity [9]. It was also demonstrated for ultrahigh-speed optical communication in the time [Time-Division multiplexing (TDM)] and frequency domains [Wavelength-Division multiplexing (WDM)]. Using the dispersion-managed soliton technique and soliton effect, the 1 Tb/s (40Gb/s × 25 channels) WDM soliton transmission and ultrahigh speed optical TDM transmission which exceeds 1Tb/s was achieved [10]. Related to the theory of active mode-locked lasers, more details will be discussed in chapter2.

Passive mode locking is an all-optical nonlinear technique capable of producing ultra-short optical pulse, without requiring any active component, such as a modulator, inside the laser cavity. Saturable absorbers have been used for passive mode locking since early 1970s. It is the sole method available for use until the invention of the additive-pulse mode locking techniques emerged. Additive-pulse mode-locking was first demonstrated in a soliton laser by Mollenauer and Stolen (1984) [11]. Subsequent

research showed that this method can be applied to non-soliton systems as well [12]. In 1992, the technique of nonlinear polarization rotation was first used in order to build passive mode-locked fiber lasers [13] and it was quickly demonstrated that stable and self-starting pulse trains of subpicosecond pulses at a 42MHz repetition rate can be generated by using this technique [14]. Moreover, ultra-short pulses less than 100fs at a repetition rate of 48MHz were obtained in a ring cavity configuration in which the net dispersion was positive [15].

As short as femtosecond pulses and stable ultrahigh-speed pulse train can be available respectively from the passive mode-locked fiber laser and the active mode-locked fiber laser. With these advantages and different characteristic, nowadays, fiber lasers have been widely used in several different areas especially for the ultrahigh-speed fiber optical communication and nonlinear optics experiments.

1.2 The motivation of research

Fiber optical transmission using a short optical pulse train is a fundamental technology in order to achieve a high-speed and long-distance global network. For ultra-high speed fiber optical communication, the characteristic of ideal transmission source is demanded to be stable (low amplitude jitter), widely tunable wavelength, transform limited, low timing jitter, adjustable pulsewidth, and high extinction ratio. Therefore, a mode-locked erbium-doped fiber lasers (ML-EDFLs) source with high repetition rate and short pulse width is good selection for ultrahigh-speed communication system. Besides, these ML-EDFLs can produce higher output power and lower insertion loss in all fiber system.

Comparing with semiconductor lasers, because of the serious chirp problem of semiconductor lasers [16], mode-locked EDFLs can easily generate transform-limited pulse trains at an ultrahigh speed repetition rate more than 10GHz. On the contrary, although semiconductor lasers can also produce very high repetition rate pulse trains, the pulse quality is typically worse and small output power. For 1550nm center wavelength, the maximum output power of semiconductor laser is about 10dBm much smaller than that of the fiber laser about 23dBm. Moreover, by using the feedback control of phase-locked loop technique, the long stability mode-locked EDFLs produced 40GHz pulse trains with ultra-short pulsewidth and wavelength tuning range from 1530 to 1560nm was successfully achieved [9].

Although passively mode-locked erbium-doped fiber lasers easily produce the femtosecond pulses needed for multigigabit communication systems, such lasers only could be operated at only a few gigabit repetition rate (<10GHz) and suffered from timing and pulse dropout or multiple pulse instabilities. Hybrid actively and passively mode-locked lasers do not possess timing problems but may still suffer from multiple

pulse production or dropout [17]. Using rational harmonics mode-locking technique can enable the use of longer cavities and slower components to generate pulses at higher bit rate, but different pulses will experience different losses in the modulator. This may lead to large amplitude fluctuations between consecutive pulses in the pulse train. The lasers utilized only active harmonic mode-locked generate one pulse in every timing window at ultra-high repetition rate, but its' pulsewidth is typically wider than passively mode-locking and hybrid mode-locking. However, it can be overcome by using additional structure such as nonlinear pulse compressing to narrow it. Therefore, one of the best choices of transmission source for ultra-high speed fiber optical communication is active mode-locked erbium-doped fiber laser.

In this study, we fabricate an actively mode-locked erbium-doped fiber laser with clean pulse, high output power, short optical pulsewidth, high repetition rate, and high SMSR. Besides, the time-bandwidth product of the laser is close to transform-limited. In the part of simulation, the experimental structure is also simulated by using the VPI.

1.3 The structure of the thesis

This thesis is consisted of four chapters. Chapter 1 is an introduction of history of fiber lasers and our motivation for demonstrating this research. In chapter 2, it will describe the theory of mode-locked fiber lasers including the active mode-locking and some methods about how to stabilize ML-EDFLs. In chapter 3, it presents experimental setup and results. Analyses of the results are also included. In chapter 4, by using VPI, the simulation results of our ML-EDFL structure are shown. It will be also compared with the results of the experiment in chapter3. Finally, in chapter 5, we make a brief conclusion and discuss results that we have successfully achieved. Some possible improvements on the laser configuration are also proposed.

CHAPTER 2

The Theory of Mode-Locked Lasers

2.1 Theory of mode-locked lasers

Two techniques used for generating short optical pulses from lasers are known as Q-switching and mode locking. Mode locking means that the phases of longitudinal modes in the laser cavity have fixed relation. In order to explain it, at first, we can assume that every optical field in the laser cavity has irregular intensity and different resonance frequencies as shown in figure 2.1. It means that the laser is not a single mode laser. [18]

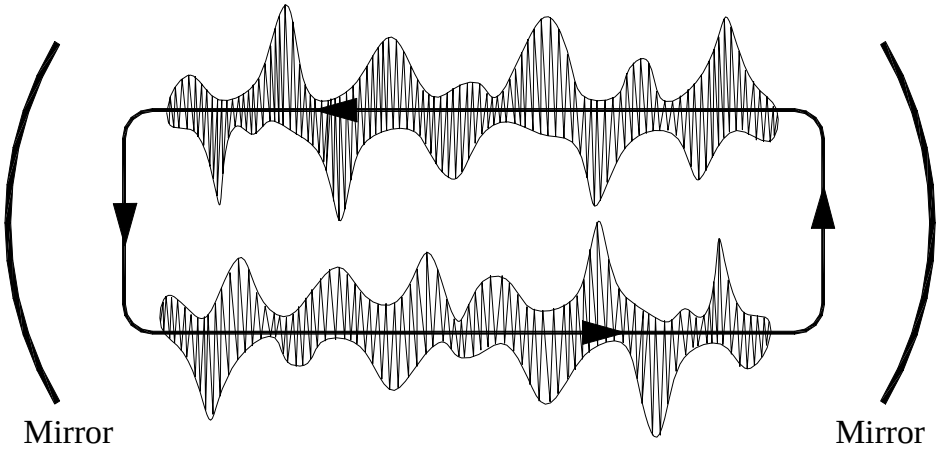

Figure 2.1 initial state of optical field in laser cavity

However, when the laser starts to become stable, there are only some modes can exist in the cavity. The output of the laser consists of these modes. These modes which can exist in the cavity are dependent on the cavity length. We could express it as following equation,

$$\Delta\omega = \omega_{q+1} - \omega_q = \frac{2\pi}{T} = \frac{\pi \cdot c}{L} \tag{2.1.1}$$

where L is cavity length. Analyzing in time domain, we assume that there are three

frequencies $\omega_q, \omega_{q+1}, \omega_{q+2}$ can exist in the laser cavity and they have the same amplitude. The interval between any two of these frequencies is $\Delta\omega$. The electron field can be expressed as

$$\varepsilon(t) = \mathrm{Re}[E_1 e^{j(\omega_q t+\phi_1)} + E_2 e^{j(\omega_{q+1} t+\phi_2)} + E_3 e^{j(\omega_{q+2} t+\phi_3)}] \tag{2.1.2}$$

The output of electric field is the function of time. The intensity can be written as following

$$\begin{aligned} I(t) \equiv |\varepsilon(t)|^2 &= E_1^2 + E_2^2 + E_3^2 + 2E_1E_2\cos[(\omega_2-\omega_1)t+\phi_2-\phi_1] \\ &+ 2E_1E_3\cos[(\omega_3-\omega_1)t+\phi_3-\phi_1] \\ &+ 2E_2E_3\cos[(\omega_3-\omega_2)t+\phi_3-\phi_2] \end{aligned} \tag{2.1.3}$$

where ϕ_1, ϕ_2, ϕ_3 are the relatively phase of these three frequencies $\omega_q, \omega_{q+1}, \omega_{q+2}$. If these phases are the function of time and their interval are not fixed, the ratio of beat frequency of these three frequencies will change in time.

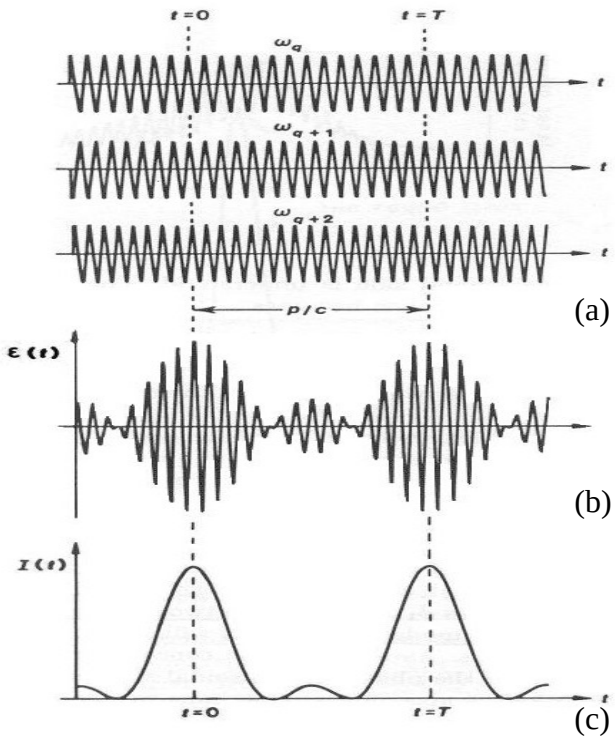

Figure 2.2 (a) the electric field of individual frequency $\omega_q, \omega_{q+1}, \omega_{q+2}$ and they have fixed relation of the phase. (b) total electric field (c) total optical field.

However, if the electric field of these three frequencies all have their maximum values at T=0 and fixed phases; we can get a periodic peak power at the output as shown in figure 2.2. The mediate figure is expressed as total electric field. The peak of the total electric field is triple times value of the single electric field. Therefore, we can extrapolate that the maximum intensity of total optical field is nine times value of the single optical field. Then, the pulse trains occur.

Analyzing in frequency domain, the distribution of electric field of one round trip time is shown as figure 2.3 (a). The range of the distribution of electric field is only in $0 < t < T$, where T is round trip time and $\varepsilon(t)$ is zero at other times. Using the Fourier transformation, it can be transformed to frequency distribution, $E(\omega)$ as shown in figure 2.3 (a) at the right hand side. Where $\varepsilon(t)$ is the pulse signal which consists of sine waves in the cavity and its pulsewidth $\tau_p << T$.

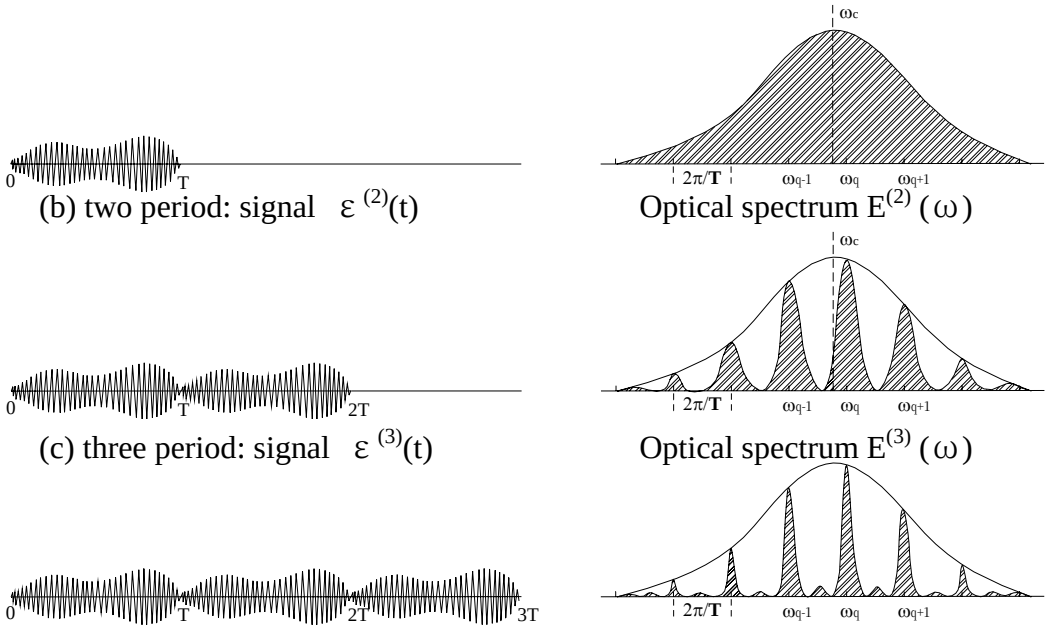

Figure 2.3 the distribution of electric field (left hand side) of once (a), two (b), three round trip times (c) of the cavity and its optical spectrum (right hand side)

In this example, we can take a notice that ω_c, carrier frequency, is unnecessary to equal to the longitudinal modes ω_q inside the cavity. The $\varepsilon^{(2)}(t)$ of two round trip time is twice reiteration of the same signal ε (t) of one round trip time. We could write it as $\varepsilon^{(2)}(t) \equiv \varepsilon(t) + \varepsilon(\tau - T)$, where T is a delay time in time domain. After Fourier transformation, $\varepsilon(\tau - T)$ is expressed as $\exp(-jT\omega) \times E(\omega)$, such that

$$E^{(2)}(\omega) = \frac{1}{2}[1 + e^{-jT\omega}] \times E(\omega) = E(\omega)\cos(T\omega/2)\exp(-jT\omega/2) \qquad (2.1.4)$$

The distribution of intensity in frequency domain could be written as

$$I^{(2)}(\omega) = \left|E^{(2)}(\omega)\right|^2 = \frac{1}{2}[1 + \cos T\omega] \times I(\omega) = I(\omega)\cos^2(T\omega/2) \qquad (2.1.5)$$

Equation (2.1.5) can be illustrated as figure 2.3 (b) at the right hand side. After more than twice of the round trip times, only frequency which is also one of the longitudinal modes of the cavity can exist in this cavity as shown in figure 2.3 (a)-(c) and the others which cannot be allowed to exist will become zero.

Fiber lasers typically operate simultaneously in a large number of longitudinal modes falling within the gain bandwidth. Therefore, the total optical field can be written as

$$E(t) = \sum_{m=-M}^{M} E_m \exp(i\phi_m - i\omega_m t) \qquad (2.1.6)$$

where E_m, ϕ_m, and ω_m are amplitude, phase, and frequency of a specific mode among 2M+1 modes. If all modes operate independently of each other with no definite phase relationship among them, the interference terms in the total intensity $|E(t)|^2$ averages out to zero. This is the situation of multimode CW fiber laser [19].

Active mode locking occurs when phases of various longitudinal modes are synchronized such that the phase difference between any two neighboring modes is locked to a constant value ϕ such that $\phi_m - \phi_{m-1} = \phi$, as we explain previously. Such

a phase relation implies that $\phi_m = m\phi + \phi_0$ which means that they have fixed phase relation. The mode frequency ω_m can be written as $\omega_m = \omega_0 + 2m\pi\Delta\nu$. If we use these relations in equation (2.1.6) and assume for simplicity that all modes in the cavity have the same amplitude E_0, we can express it analytically. The total intensity is given as

$$|E(t)|^2 = \frac{\sin^2[(2M+1)\pi\Delta\nu t + \phi/2]}{\sin^2(\pi\Delta\nu t + \phi/2)} E_0^2 \qquad (2.1.7)$$

It is a periodic function of time with period $\tau_r = 1/\Delta\nu$, which is just the round trip time inside the cavity. ϕ is the phase difference between any two neighborhood modes. The simulation of the total intensity $|E(t)|^2$ is shown in figure 2.4 for nine coupled modes (M=4).

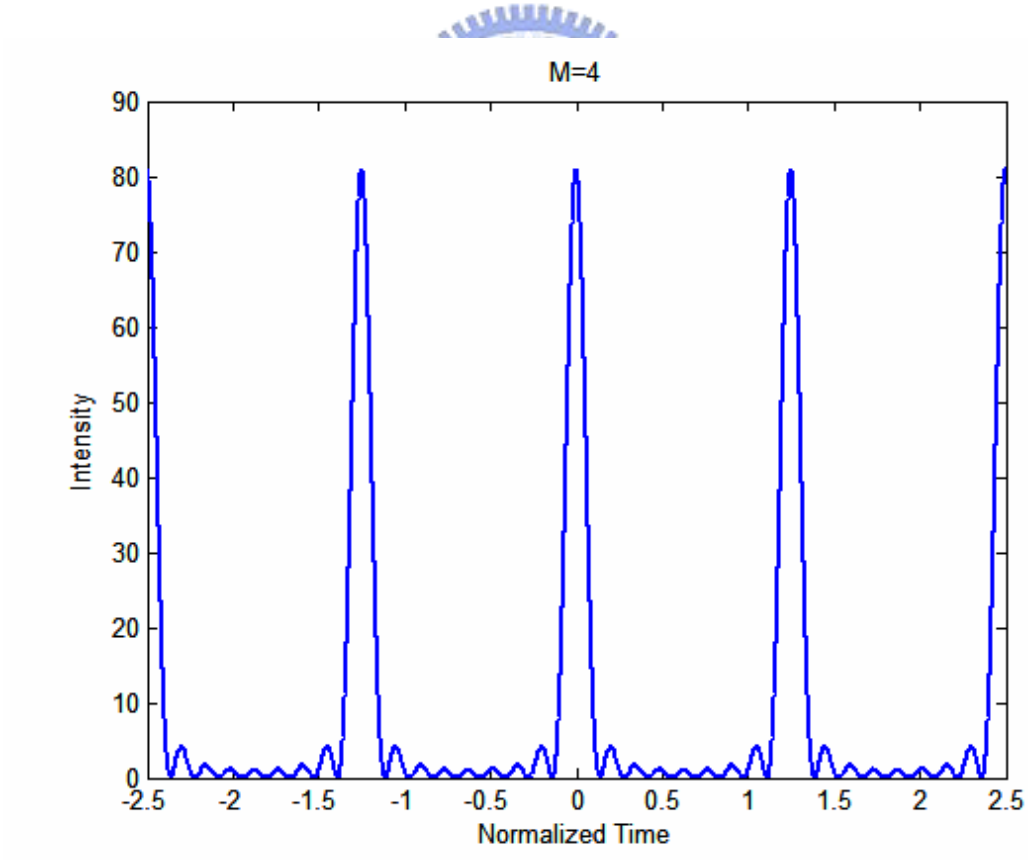

Figure 2.4 Illustration of the mode-locked pulse train as M=4

Typically, mode-locked laser could be distinguished into active mode-locked laser and passive mode-locked laser. The generation of femtosecond short pulses could be easily made by passive mode–locked laser using nonlinear effect in the cavity. There are many kinds of passive mode-locking which can be used, such as mode-locking with slow or fast saturation absorber [20], additive pulse mode-locking (APM) [21], nonlinear polarization rotation mode-locking (P-APM) [22], and Kerr lens mode-locking (KLM) [23] etc la.

Active mode locking could be achieved through directly modulation of the intensity or phase of light by using the active components, such as Electro-Optical modulator and acoustic-optical modulator. It will be discussed more details in following section 2.2. Beside, to overcome the influence of thermal and environmental perturbation becomes more and more important for a short pulse and high repetition rate fiber laser used for optical communication system. In order to increase the bit error rate (BER), it is necessary to decrease the timing jitter and amplitude jitter of fiber laser, especially operating at ultra-high repetition rate. Therefore, we will discuss how to stabilize the active mode-locked fiber laser in section 2.3.

2.2 Active mode-locked lasers

2.2.1Amplitude modulation mode-locking

Amplitude modulation mode-locking is a method to produce a short pulse train and high repetition rate by directly modulating the optical amplitude of the light. It can be analyzed both in the time and frequency domains [24].In the time domain, the amplitude modulation provides a time dependent loss so that only the pulses which pass through the modulator at the lowest loss will exist. As the pulses pass through the modulator continually, the pulsewidth will get shorter and shorter. However, shorter pulses will experience larger dispersion and finally the two forces balance each other to form the steady state pulse shape. In this way, the modulation time period must be equal to a multiple of the roundtrip time for producing stable pulses. Figure 2.5 shows the active mode-locking process in the time domain.

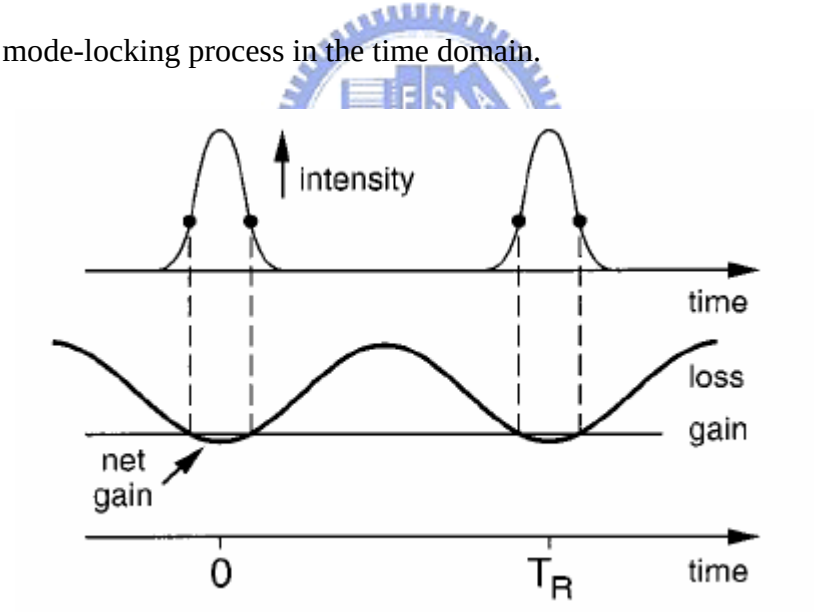

Figure 2.5 Principle of active mode-locking explained in the time domain [24]

In frequency domain, we can assume that the center frequency of signal gain profile is ν_0, and the amplitude of the central mode without amplitude modulation is expressed as $\varepsilon(t) = E_0 \cos(\omega_0 t)$. The transform function of the active amplitude modulator, which controls the loss of light in the cavity, can be written as

$\tilde{t}_{am} = \exp[-\Delta_m(1-\cos\omega_m t)] \cong \exp[-\frac{1}{2}\Delta_m\omega_m^2 t^2]$, where $\omega_m = 2\pi f_m = 2\pi N\Delta f$ and f_m is modulation frequency, such as the signal after modulation can be expressed as following,

$$\begin{aligned} E(t) &= (1+\Delta_m\cos\omega_m t)E_0\cos\omega_0 t \\ &= E_0\cos\omega_0 t + E_0\frac{\Delta_m}{2}\cos(\omega_0+\omega_m)t + E_0\frac{\Delta_m}{2}\cos(\omega_0-\omega_m)t \\ &= E_0\cos\omega_0 t + E_0\frac{\Delta_m}{2}\cos 2\pi(\nu_0+f_m)t + E_0\frac{\Delta_m}{2}\cos 2\pi(\nu_0-f_m)t \end{aligned} \quad (2.2.1)$$

where Δ_m is modulation index. It is clear from this equation that the center frequency ν_0 induces two side modes with fixed phase relationship $(\nu_0 \pm f_m)$ while it experiences modulation of active modulator. Similarly, after these two side modes which are made by center frequency ν_0 go through the active amplitude modulator, there will also increase other new side modes $(\nu_0 \pm 2f_m)$ with fixed phase relationship. These sidebands can injection-lock the neighboring modes sequentially and finally the mode-locking is achieved. (See figure 2.6)

The modes that are separated every f_m will be phase-locked, and short pulses can be formed in the time domain. When N equals to 1, the laser is mode locked at the fundamental repetition rate. When N is an integer greater than 1, the laser is harmonic mode locked. We will discuss it detailed in the following section. (See section 2.2.3)

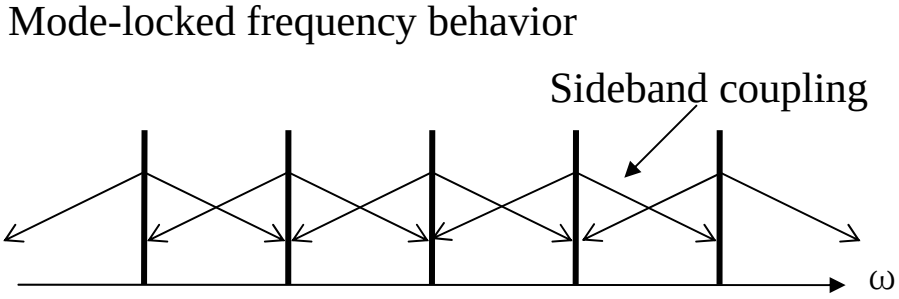

Figure 2.6 Principle of actively mode-locking explained in the frequency domain

2.2.2 Phase modulation mode-locking

Phase modulation mode-locking is a method to produce a short pulse train by modulating the optical phase. It can also be analyzed both in the time and the frequency domains [25].

In the time domain, the phase modulator provides a periodic phase change for the optical pulse. If the pulsewidth is much smaller than the modulation period, the change of the optical phase produced by the phase modulator can be expressed as:

$$\phi(t) = \phi_0 + \frac{d\phi}{dt}t + \frac{d^2\phi}{dt^2}t^2 + \ldots \qquad (2.2.2)$$

where ϕ_0 is a constant phase, and the influence of ϕ_0 on optical pulse can be neglected . The first order term $\frac{d\phi}{dt}$ will influence the central frequency of the pulses and shifting magnitude of influence depends on its value. Therefore, if $\frac{d\phi}{dt}t \neq 0$, the central frequency of optical pulse will be changed. In another word, the pulse will experience smaller gain and center frequency will still be changed, if $\frac{d\phi}{dt}t$ is still not equal to zero. This is unstable and will not lase. Only the pulses which pass through the PM modulator and experience maximum gain is at $\frac{d\phi}{dt}t = 0$, and its every round trip is able to be stable. Then, it will lase. (See figure 2.7)

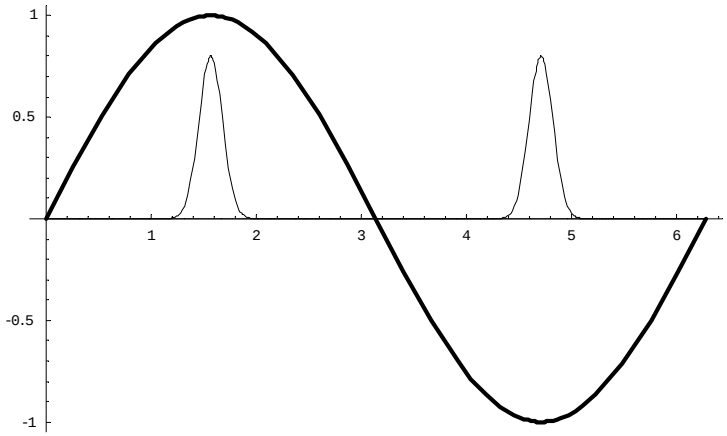

Figure 2.7 Time domain of phase modulation

As regarding the second order term $\frac{d^2\phi}{dt^2}t^2 \equiv \eta t^2$, it adds a chirp to the pulse. Also, it will affect the optical bandwidth of the pulses. The effect can be expressed in mathematics by:

$$\Delta\omega = \sqrt{\frac{1}{\tau^2} + \eta\tau^2} \tag{2.2.3}$$

where $\Delta\omega$ is the bandwidth of optical pulse, τ is the pulsewidth, and $\eta = \frac{d^2\phi}{dt^2}$ is the chirp parameter.

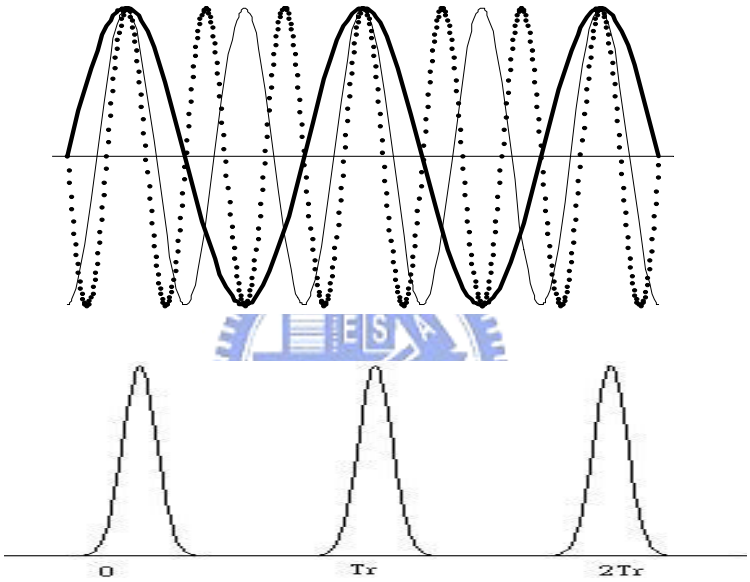

Figure 2.8 Development of pulse train in time domain by superposition of modes

In the frequency domain, we can assume that the central frequency is ν_0. When it passes through the phase modulator, the electric field of the pulse can be written as:

$$\begin{aligned} E(t) &= E_0 \cos(2\pi\nu_0 t + \Delta_m \cos(2\pi f_m t)) \\ &= E_0 \sum_{-\infty}^{\infty} J_n(\Delta_m) \cos(2\pi\nu_0 + n2\pi f_m)t \end{aligned} \tag{2.2.4}$$

where f_m is the modulating frequency of phase modulator, Δ_m is the modulation index, and J_n is the n-th order Bessel function. If ν_0 is one of the harmonic modes in the laser cavity and f_m is N times magnitude of the fundamental harmonic

frequency of the cavity, these harmonic modes ($\nu_0 + Kf_m$) will have the fixed phase relation with the ν_0, where K=±1, ±2, ±3, , ,etc la. Therefore, all these harmonic modes will have fixed phase relation. In time domain, these harmonic modes will create constructive interference at periodic time and destructive interference at other times by injection-locking. (See figure 2.8)

2.2.3 Harmonic mode-locking

A continuous wave erbium ring laser can be actively mode-locked by using an amplitude or phase modulator to generate pulses at the modulation frequency f_m

$$f_m = f_c \tag{2.2.5}$$

$$f_c = \frac{c}{2nL} \tag{2.2.6}$$

where f_c is the cavity mode-spacing frequency, c is the speed of light, L is the cavity length and n is the refractive index of the cavity. These pulses have a round trip time of t_r, which is related to f_c and the pulse width τ as following,

$$t_r = \frac{2nL}{c} \tag{2.2.7}$$

This is known as fundamental mode-locking, and it produces pulses at repetition rate equal to f_c.

The cavity mode-spacing frequency of a typical laser cavity is of the order of 0.5~6MHz. To increase the pulse repetition rate, pulses could be produced at integer harmonics of the cavity mode-spacing by modulating at a frequency f_m, given by

$$f_m = Pf_p \tag{2.2.8}$$

where P is an integer representing the number of longitudinal modes locked, and ranges from a few hundred to tens of thousand. This is known as harmonic mode

locking, these longitudinal modes with equal interval Pf_p is called as supermodes, and its new round trip time shows as following,

$$t_r = \frac{2nL}{c} \cdot \frac{1}{P} \tag{2.2.9}$$

In 1970s, the KS (Kuizenga and Siegman [26]) theory predicted that with amplitude mode-locking the time bandwidth product is 0.441 for a chirp-free Gaussian pulse and 0.315 for a Sech^2 pulse. Furthermore, it states that the pulsewidth τ is inversely proportional to $(\delta)^{1/4}$ and $(f_m \cdot \Delta f_{3dB})^{1/4}$, so that

$$\tau = K \cdot \left(\frac{1}{f_m \cdot \Delta f_{3dB}} \right)^{\frac{1}{2}} \cdot \left(\frac{1}{\delta} \right)^{\frac{1}{4}} \tag{2.2.10}$$

where δ is the effective single-pass amplitude modulation depth, Δf_{3dB} is the 3dB gain band width of the laser cavity and K is a pulse shape-dependent constant. It is clear from this equation that with increasing modulation frequency and increasing modulation amplitude, the optical pulsewidth will be narrowed.

However, though we can use this way to promote higher repetition rates, the drawback of harmonic mode-locking is not stable for a long time. We will discuss it later.

Actually, the smallest pulsewidth and chirp of the pulses can be estimated by using the time-bandwidth product of transform limited. For chirp free Gaussian sharp, time bandwidth product is 0.441. For Sech^2 sharp, time bandwidth product is 0.315. We can use this transform-limited to appraise our laser. However, the exact estimate is not possible since the cavity dispersion is not considered in equation (2.2.10).

2.2.4 Rational harmonic mode-locking

Using mode-locked fiber ring laser to generate pulses at very high repetition rates requires a small cavity path length and high-speed modulators and signal generators, because of long cavity length. An alternative solution is using a rational mode-locking technique to generate pulses at rational harmonics of the fundamental locking frequency, thus enabling the use of longer cavities and slower components to generate pulses at higher bit rate [27].

Ahmed and Onodera [28] introduced the idea of mode-locking a laser cavity at rational harmonics of the modulator frequency in order to generate pulses at a repetition rate higher than the modulator frequency. This is achieved by slightly detuning the cavity frequency f_c so that it is now related to the modulator frequency f_m expressed as following equation (2.2.11),

$$f_m = \left(p \pm \frac{1}{k} \right) \cdot f_c \tag{2.2.11}$$

where k is the rational number which can have values range from 1 to no more than 20. This leads to a pulse repetition rate of f_p, given by

$$f_p = (kp \pm 1) \cdot f_c \tag{2.2.12}$$

Therefore, rationally mode-lock ring lasers generate optical pulses at a repetition rate which is k times value of the modulation frequency.

Rational mode-locking of erbium-doped fiber lasers at repetition rate of up to 200GHz have been reported [29], using values of k as high as 15. Actually, when k $\geqq$ 3, problems arise because different pulses experience different losses in the modulator. This may lead to large amplitude fluctuations between consecutive pulses in the pulse train. These fluctuations greatly increase the error rate and are not tolerable in optical communication systems.

2.3 Stabilization of mode-locked laser

A stable optical short pulse source with a high repetition rate is very important to ultrahigh speed optical communication. The active mode-locking of erbium-doped fiber lasers is one of the most attractively potential ways of achieving this, because it can produce a transform-limited, picosecond pulse train with ultrahigh repetition. However, problems arise with fiber lasers due to their susceptibility to mechanical vibrations and temperature variations affecting the length of the fiber cavities. The resulting instability and the difficulty of tuning the repetition frequency have been the major barriers to the application in communications where minor perturbations can cause intolerable bit errors, especially operating at ultra-high speed repetition rate. Therefore, the additional scheme of stability of mode-locked fiber laser becomes necessary.

2.3.1 Regenerative mode-locking

The cavity length in an actively mode-locked fiber laser is typically much longer than that of other mode-locked lasers. When a small perturbation is applied to the cavity, the absolute frequency compared with that in ordinary lasers will change. This means that it is difficult to maintain the optimum operational conditions over a long period, although it is possible to generate clean short pulses in a short period.

Also, this problem can be overcome with a regenerative mode-locking technique [30]. The regeneratively mode-locked fiber laser has long term stability since the modulation frequency is extracted from the mode-locked pulse itself. The structure is shown as figure 2.9. Regenerative mode-locking is accomplished by feeding back the longitudinal self-beat signal which is detected by a high speed photodetector and a high Q filter. Because the phase between the pulse and the modulation signal is adjusted, the pulses will always experience maximum transmission when they pass

through the modulator. Thus, complete mode-locking is achieved automatically because the ideal feedback signal, which reflects the instantaneous frequency change between the longitudinal beats, is used as the modulation frequency even when some perturbation are applied.

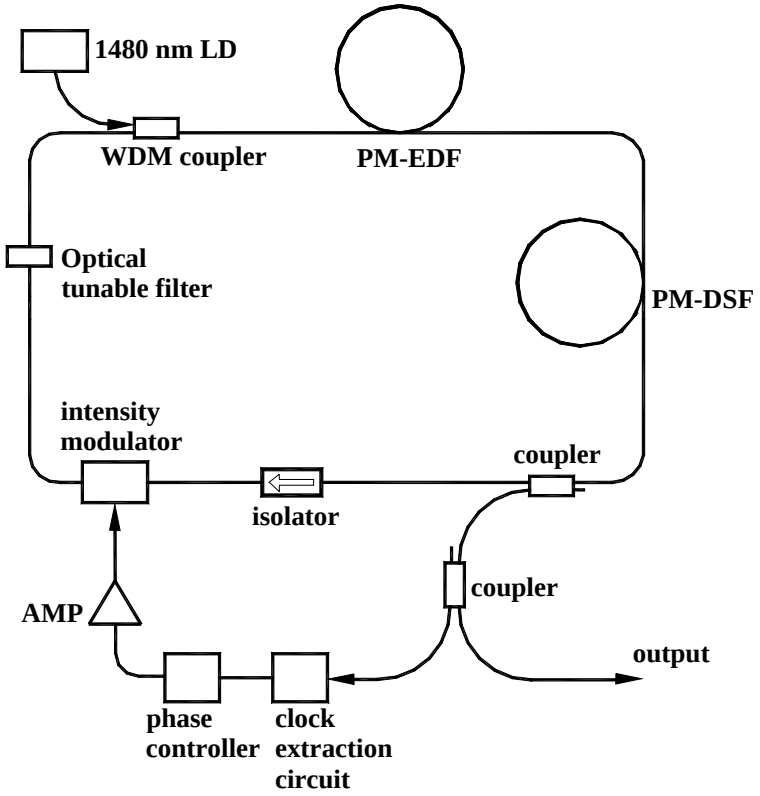

Figure 2.9 Experimental setup for the harmonically and regeneratively mode-locked erbium-doped fiber laser [30].

Actually, regenerative mode-locking has several similarities to passive mode-locking. Lasing is initiated by the noise through the use of artificial loss modulation, and the technique automatically adjusts the modulation frequency as the cavity length changes. However, the technique has one drawback in that the repetition rate fluctuates with time in a free running condition when the optical path length in the cavity is not stable. Therefore, it is necessary to have another mechanism to stabilize the repetition rate of the regeneratively mode-locked fiber laser at the fixed frequency, such as phase-locked loop.

2.3.2 Phase-locked loop (PLL)

In 1992, for active mode-locked fiber laser, the stabilization mechanism used relied on locking the electrical phase of output optical pulse to that of the drive source have been demonstrated [7]. To stabilize the laser, they developed the phase-locking circuit shown within the dashed line. (See figure 2.10)

A length of erbium-doped fiber wound on a piezoelectric crystal (PZT). It works as voltage control oscillator (VCO). A fraction of the laser output is detected by a photodiode, amplified and filtered with a narrow bandwidth filter to generate a sinusoidal signal. The frequency mixer work as a phase detector which compares the phase of the pulse train and that of the drive source (synthesizer). The error signals will occur from the mixer while there are influences affecting the fiber cavity with time. Simultaneously, the displacement of the PZT which was controlled by error signals feedback adjusts the length of the fiber cavity to compensate the perturbation of the fiber cavity caused by mechanical vibrations or temperature variations.

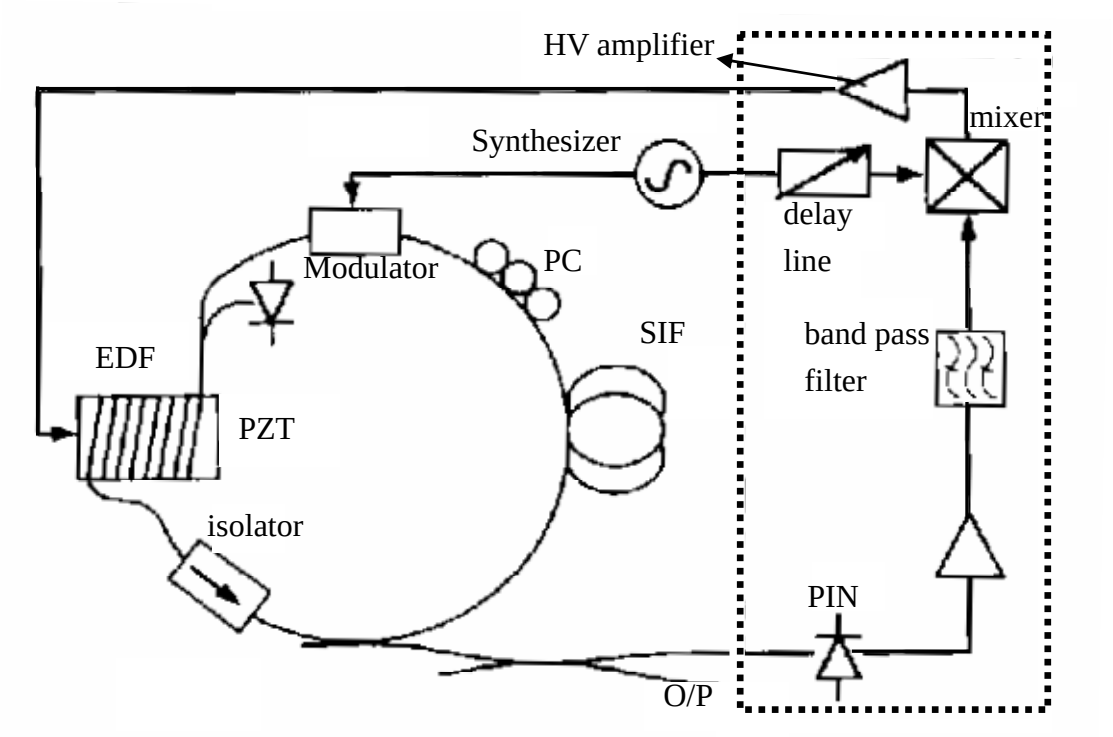

Figure 2.10 Mode-locked Erbium-doped fiber ring laser and stabilization scheme (Dashed line), where “PC” is polarization controller and “SID” is step index fiber [7]

In this paper, once the output pulse is locked in this way, it is possible to tune the synthesizer by ±5~6 KHz with a very little change in either pulsewidth or bandwidth. Actually, this tuning range corresponds to the change of the fiber length wound on PZT, which is also limited by the amplifier output voltage range. Besides, the speed of the phase-locking circuit is limited by the response of the high voltage amplifier. As a result, only thermal drifts and vibrations of a few hundreds of Hertz can be effectively suppressed. However, it is enough to overcome the influence of generally environmental perturbation to the fiber laser.

Recently, in order to stabilize mode-locked fiber laser with ultra-high speed repetition rate used for communications, phase-locking technology is publicly used. It is also utilized in regeneratively mode-locked fiber laser to stabilize its repetition rate [9].

CHAPTER 3

Experimental Setup and Results

3.1 Introduction of the experiment

The basic experimental setup is shown as figure 3.1. This fiber laser consisted of a polarization-maintaining erbium-doped fiber (PM-EDF), a WDM coupler, a 10 % coupler, a polarization-maintaining (PM) isolator, a $LiNbO_3$ intensity modulator, and a tunable optical bandpass filter. The electro-optical (EO) intensity modulator is put into the fiber ring cavity in order to achieve active mode-locking. As shown in the figure 3.1, the method of forward pumping was utilized in this experimental setup, and about 100mW of 980nm pumping laser diode was available in the experiment. Operating current versus output power of the pumping diode is shown as figure 3.2(a). Figure 3.2(b) is shown the optical spectrum of the pumping laser diode operating at 200mA. It was pumping into the cavity through the flex core fiber of WDM coupler.

The gain profile of the PM-EDF is shown as figure 3.3. The higher repetition rate of mode-locked fiber laser was operated, the more serious of polarization fluctuation it suffered. Therefore, most of fibers in the cavity were polarization-maintaining fiber in order to prevent polarization fluctuation. Besides, in active mode-locked laser, RF signal which drives the modulator is generated by a stable synthesizer at a fixed frequency in order to obtain the phase matching between the modes.

The polarization-maintaining isolator, which is also polarization dependent, is inserted in the cavity to ensure the optical pulses propagating in unidirectional operation. Besides, it is placed between the optical tunable filter and PM-EDF in order to minimize the reflecting light from the optical tunable filter to the PM-EDF.

The wavelength tuning range of the band pass filter is from 1530nm to 1570nm, and its bandwidth is about 0.582nm as shown in the figure 3.4. It was measured by using broad-band white LED. Most of connections between devices in the cavity are connected by FC/APC connectors. Alternatively, some are using SUMIOFCAS 35SE-RC fusion splicer to splice these polarization-maintaining fibers.

About the EO modulator, we use one modulator to operate at 2GHz and 10GHz, and another modulator is utilized to operate at 10GHz, 20GHz, and 40GHz. More detail will be reported latter. Because of using different modulators operated at different modulation frequencies, it will be separated from two parts to analyze. At the first part of the experiment, we use the 12.5GHz JDSU modulator to operate at 2GHz and 10GHz. At the second part of the experiment, we use the 40GHz EO-SPACE modulator to operate at 10GHz, 20GHz, and 40GHz. The specifications of devices used in the fiber ring cavity are listed in table 3.1.

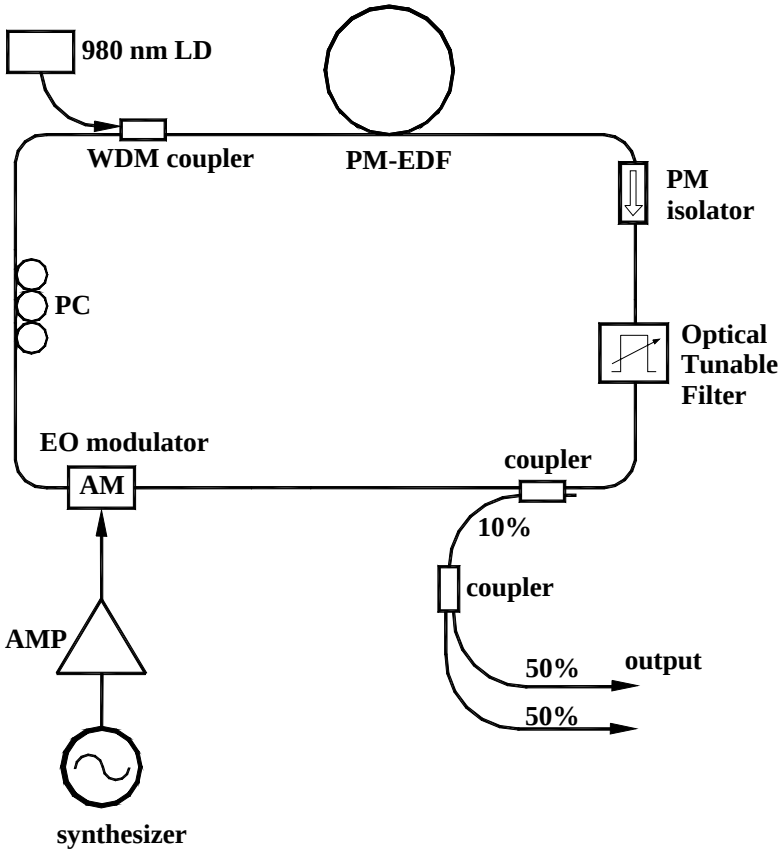

Figure 3.1 The experimental setup, where "PC" is polarization controller.

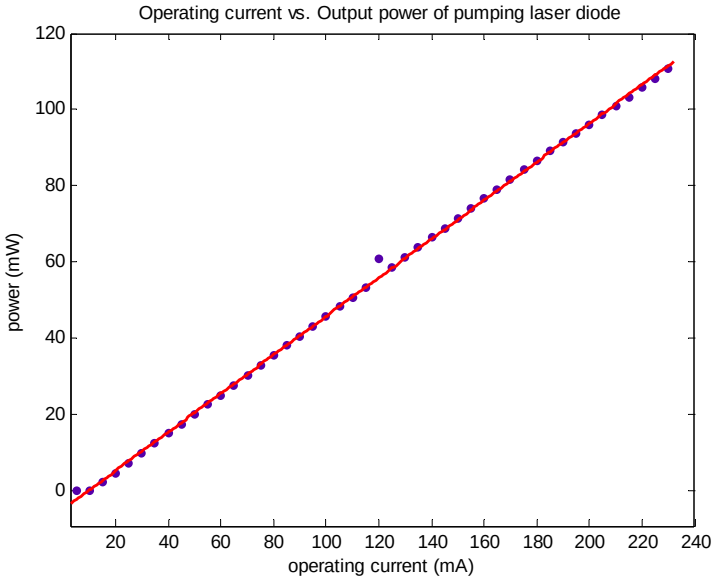

(a)

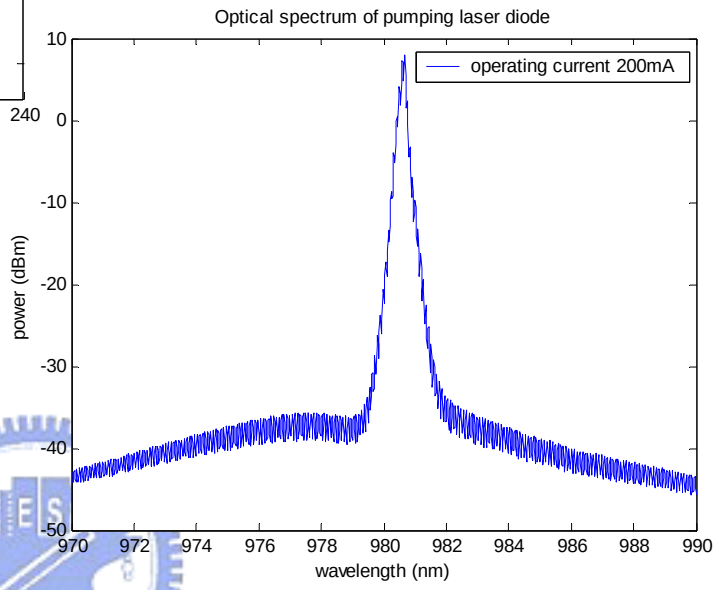

(b)

Figure 3.2 (a) Operating current versus output power of the pumping laser **(b)** Optical spectrum of pumping laser diode operated at 200mA

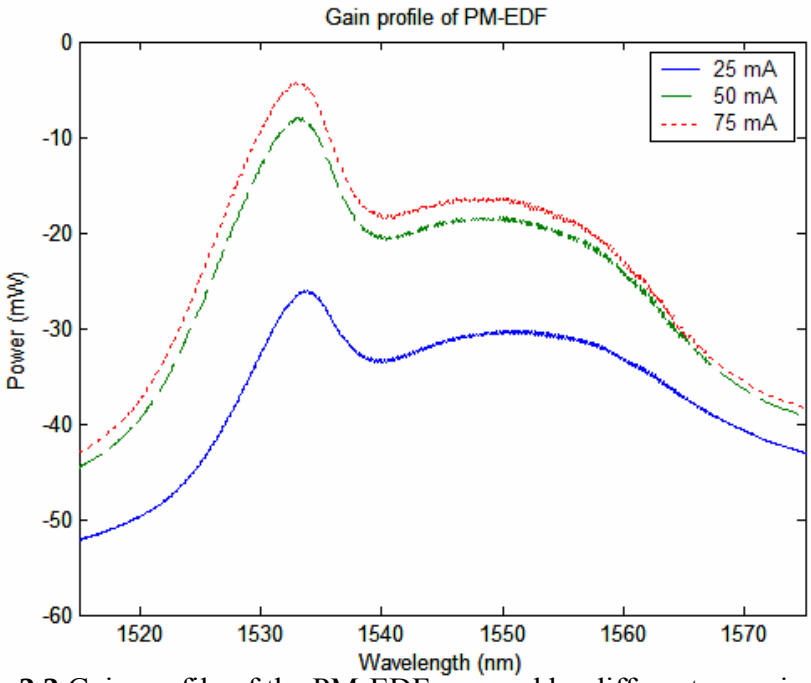

Figure 3.3 Gain profile of the PM-EDF pumped by different pumping power

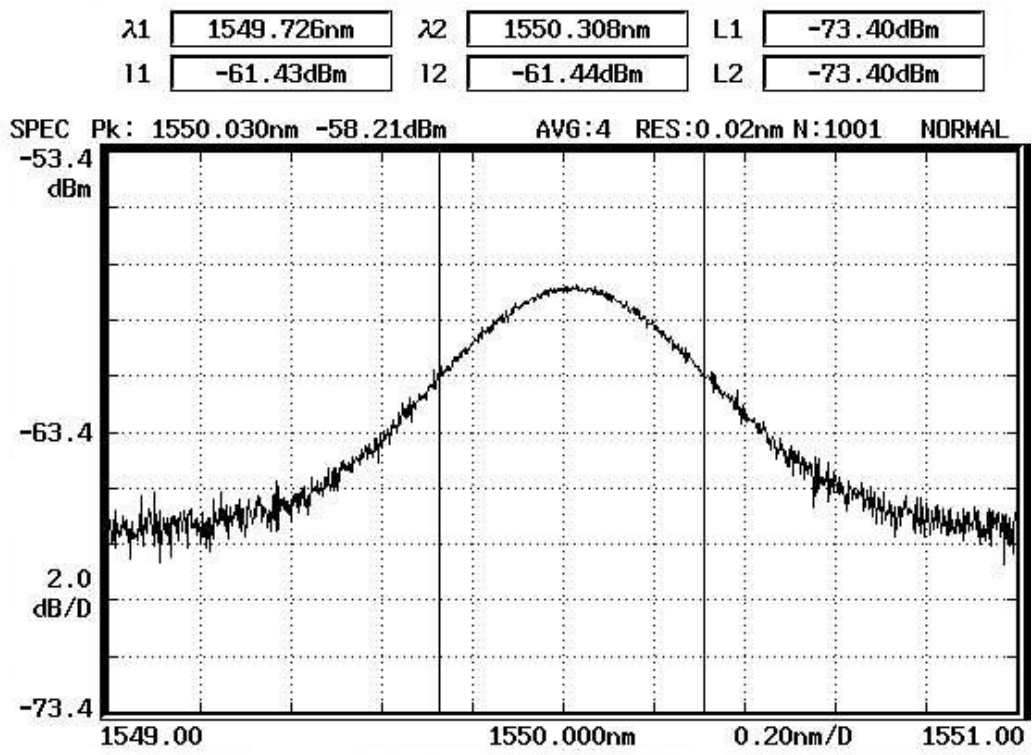

Figure 3.4 3dB bandwidth of the optical tunable filter (center wavelength at 1550nm)

component	specification
980nm pumping laser	Max power :180mW (JDSU 2700 series)
JDSU Amplitude Modulator (operating at 2GHz and 10GHz)	PM input、SM output Insertion loss : 5.5 dB V_π : 5.5V
EO*space* Intensity modulator (operating at 10GHz、20GHz and 40GHz)	PM input、PM output Insertion loss : 3.0 dB V_π : 5.2V @ 1GHz
PM Erbium doped fiber	Fiber length : 18m Attenuation : 2.50 dB/m @ 980nm 1.82 dB/m @ 1550nm
PM WDM coupler (980/1550)	Insertion loss：2 dB @ 980nm (flex core) 1 dB @ 1550nm (Panda)
PM Coupler	Output Split ratio：90/10
PM Isolator	Insertion loss：0.75dB Isolation ≧ 55 dB @1550nm Return loss ≧ 60 dB
Polarization Controller (PC)	Agilent 8169A
Optical Tunable Bandpass Filter	Bandwidth : 0.582nm @1550nm Tuning range : 1530nm ~ 1570nm

Table 3.1 The specifications of devices used in the fiber ring cavity

3.2 Setup of the experiment (Operating at 2GHz and 10GHz)

The setup is shown as figure 3.5. The 12.5GHz JDSU amplitude modulator is utilized to operate the mode-locked erbium-doped fiber laser (ML-EDFL) at 2GHz and 10GHz. The fibers in the cavity are all polarization-maintaining fibers except for the output of the modulator (the dash line in the figure 3.5). A length of the signal mode fiber (SMF) in the cavity is about 1 m. Because most of the fibers in the cavity are PM fiber, the stability of the output pulse train is sensitive to that of the polarization state in the laser cavity. Therefore, any fluctuations in this unavoidable signal mode fiber will cause serious instability of the laser output pulse.

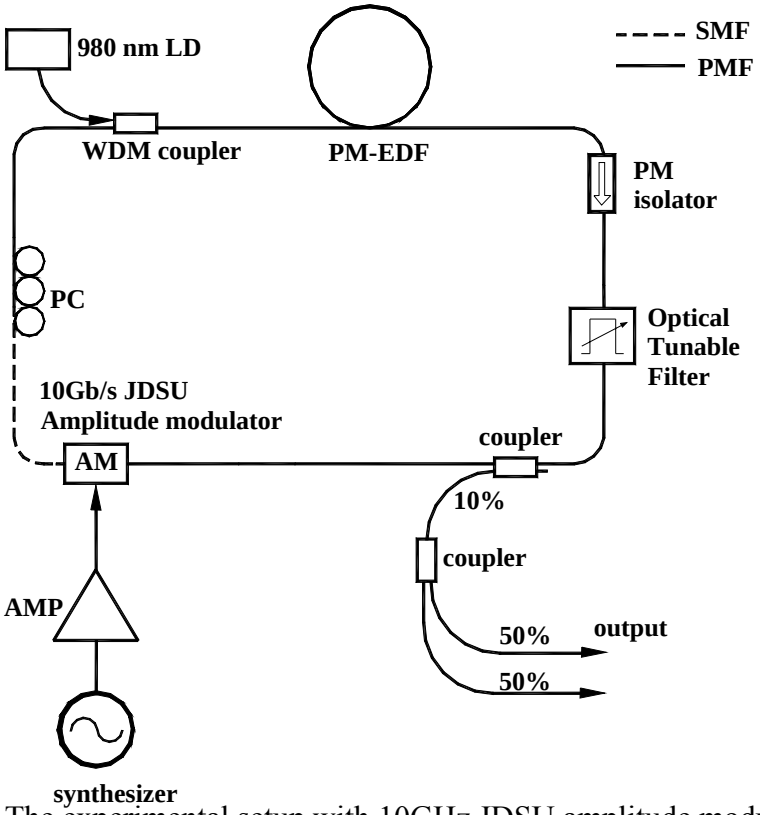

Figure 3.5 The experimental setup with 10GHz JDSU amplitude modulator

Besides, the power will also become unstable with time as shown in the figure 3.6. Its' supermode suppression ratio (SMSR) is smaller than 30dB. In order to solve this problem, a polarization controller (PC) is placed after this length of the single mode fiber. This digital polarization controller is Agilent 8169A. Agilent 8169A

consists of a polarizer, a half-wave plate, and a quarter-wave plate. The polarization state of signals pass through it can be described by the position of Poincare sphere. Therefore, after consecutive pulses propagate through this section, 8169A can be utilized to compensate the change of polarization state caused by SMF.

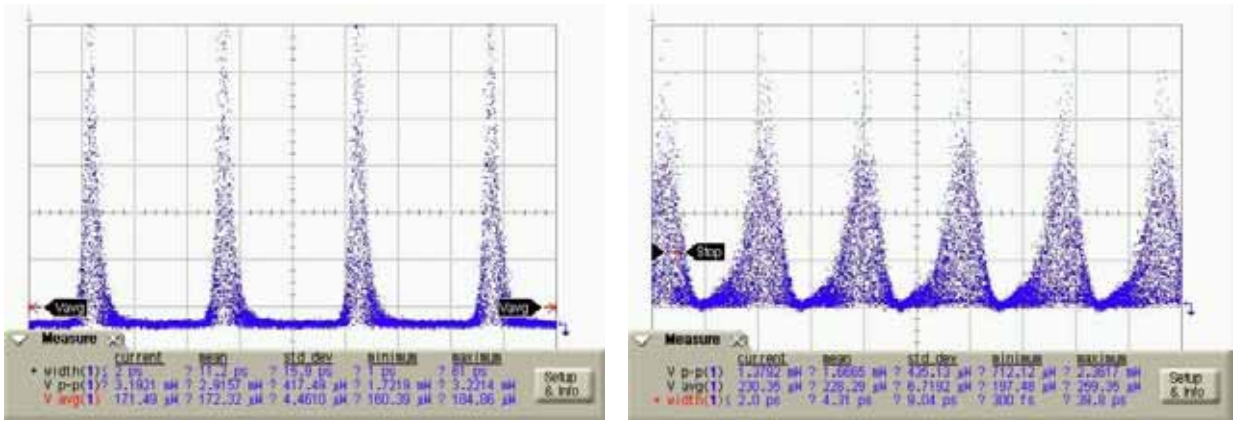

(a) (b)

Figure 3.6 (a) output of laser operated at 2GHz without polarization controller.
(b) output of laser operated at 10GHz without polarization controller.

3.2.1 Operating at 2GHz

The cavity length is about 39m and its' fundamental repetition rate is about 5.12MHz. With the digital polarization controller, the state of polarization of pulses through SMF is compensated. The output of the pulse train is very stable and clean as shown in the figure 3.7. It is measured by Agilent 86105A in different time window spans. The optical channel unfiltered bandwidth of 86105A is 15GHz, and transition time is 32ps (FWHM). The output pulsewidth of the laser is about 52ps, and the optical spectral bandwidth is about 0.066nm which is shown in figure 3.8. The time-bandwidth product is 0.429, which means that the output pulses are transform-limited and the waveform is like sech^2 shape more than Gaussian shape. With 80mW pumping power, the average output power of the laser is about 0.19mW and peak power is about 1.5mW. The RF spectrum is shown in figure 3.9, and the supermode suppression ratio (SMSR) is above 55dB. The span of left figure is

20MHz, and another is 500MHz. The parameters of the mode-locked laser operated at 2GHz repetition rate are listed in Table 3.2.

Input parameters	
980nm pump:	80 mW
cavity length:	39 m
mode spacing:	5.12 MHz
repetition rate:	2 GHz (about 400th harmonic)
modulation strength	17 dBm
Results	
central frequency:	1550.12 nm
SMSR:	> 55 dB
output average power:	0.19 mW
output peak power:	1.5 mW
optical spectrum bandwidth:	0.066 nm
Pulse width (FWHM):	52 ps
time-bandwidth product:	0.429

Table 3.2 Parameters of the mode-locked laser operated at 2GHz repetition rate

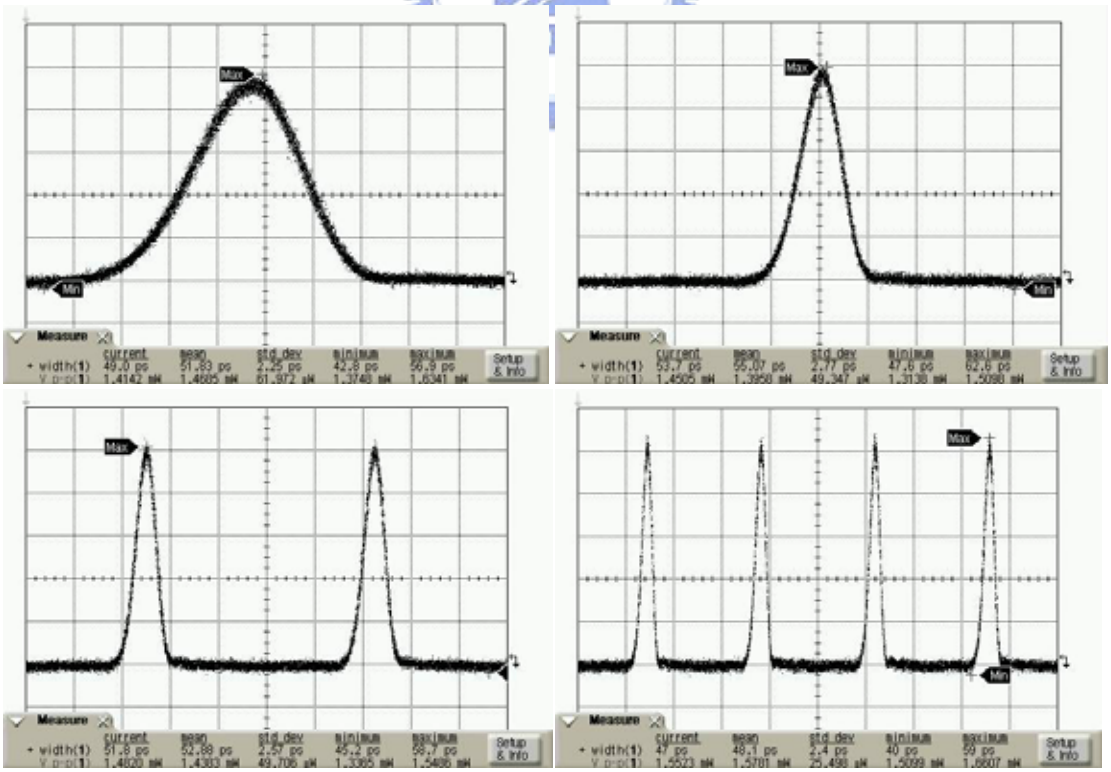

Figure 3.7 The waveform operated at 2GHz is measured by Agilent 86105A in different time window spans.

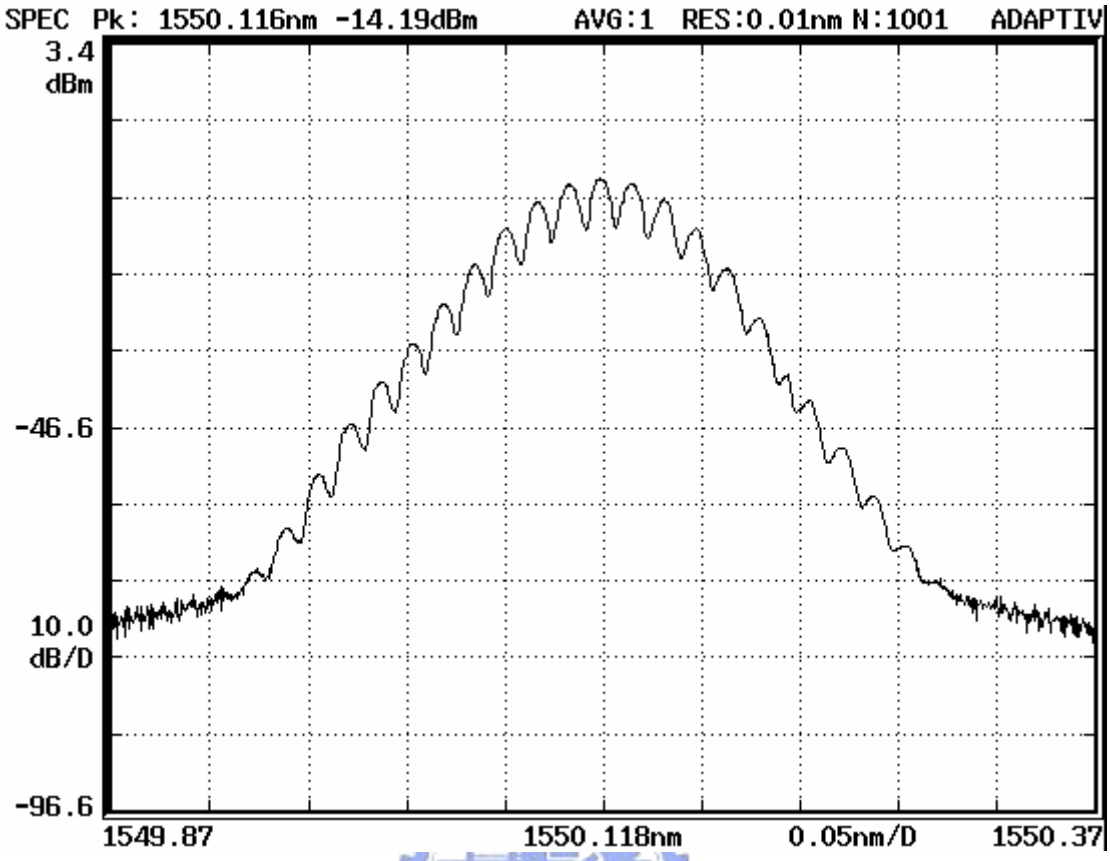

Figure 3.8 Optical spectrum

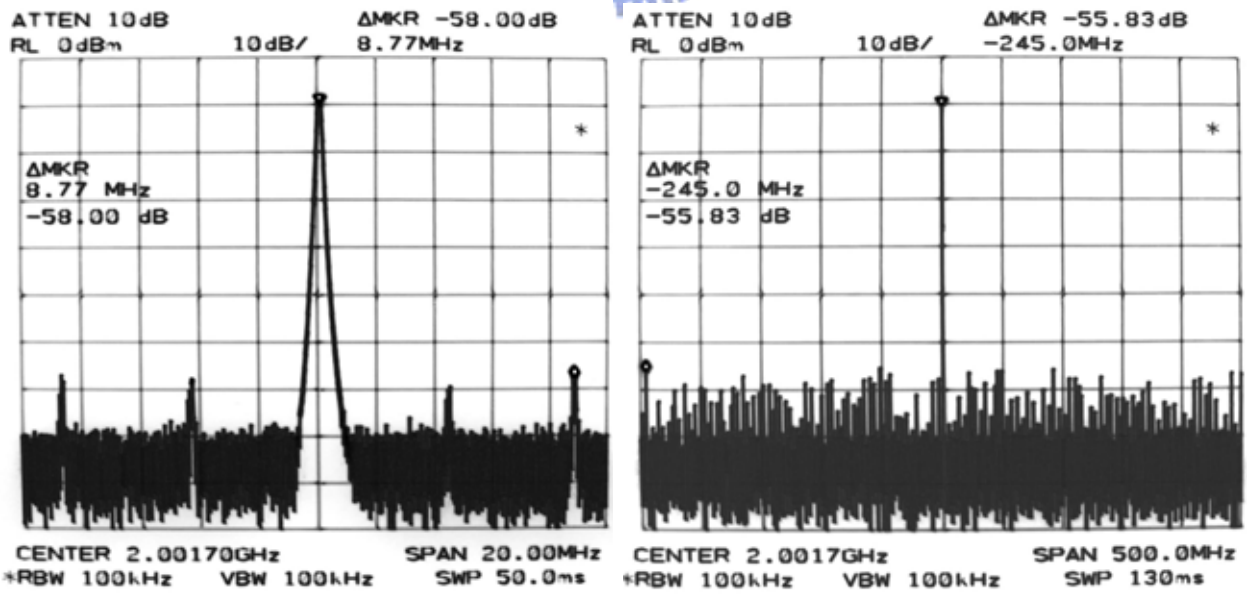

Figure 3.9 RF spectrum **(a)** span: 20MHz, SMSR: 58dB

(b) span: 500MHz, SMSR: 55dB

It is worth to mention that the pulsewidth of laser can be adjusted by using the polarization controller to change the state of the polarization in the cavity. The pulsewidth can be controlled from 82ps to 39ps, which is shown in figure 3.10 measured in the same scale. Actually, according to equation (2.2.10), the pulsewidth is unconcerned with pumping power. However, if the pulse is forming soliton ($sech^2$ shape), the situation will become different. Thus, the pulsewidth is changed while various pumping power [30]. It will be discussed detailed in following section 4.2.

Here, the mechanism was achieved by using the polarization dependent isolation and polarization dependent gain effect in the cavity. It made those different states of polarization experience different gain and loss. Besides, it is well known that the cavity which consists of all polarization-maintaining fibers is much more sensitive to the polarization state than that consists of all single mode fibers. After passing through the polarization-maintaining EDF, small core area, the state of the polarization which gets higher gain and lower loss will cause higher nonlinear effect. This nonlinear effect can shorten the pulsewidth in the ring cavity. In contrast, the state of the polarization which gets lower gain and higher loss will not cause nonlinear effect. Pulse shortening will not occur.

Some above-mentioned considerations are supported by reference [30]. Moreover, the experimental time-bandwidth product, 0.426, is smaller than the transform-limited for Gaussian shape, which means that the waveform is like $sech^2$ shape more than Gaussian shape. It can be proved by measuring the average power of different pulsewidths. The shorter pulsewidth was measured higher average power. The wider pulsewidth was measured lower average power. In the same way, it was also proven by increasing the pumping power. As the pumping power was increased, the pulsewidth was shortening. But, the adjustable range in this way is not as large as using the polarization controller.

Unfortunately, although the pulsewidth can be controlled by the polarization controller, the most stable polarization state for the cavity is only linear polarization which is on the slow axis of the fiber. Other states of the polarization are all unstable to the cavity, and their pulsewidth were changing with time. Here, the most stable pulsewidth is about 52ps and it can maintain this form above 40 minutes.

Using the optical band pass filter, the wavelength was tunable from 1530 to 1570nm. The most stable pulsewidth is about 50ps. Because of the smaller gain of EDF and higher fiber loss at these side wavelengths, the average power and peak power were smaller than that at 1550nm pumped by the same pump power. Therefore, although the pulsewidth were also adjustable by using polarization controller at these wavelengths, the tuning range is smaller than that operated at 1550nm.

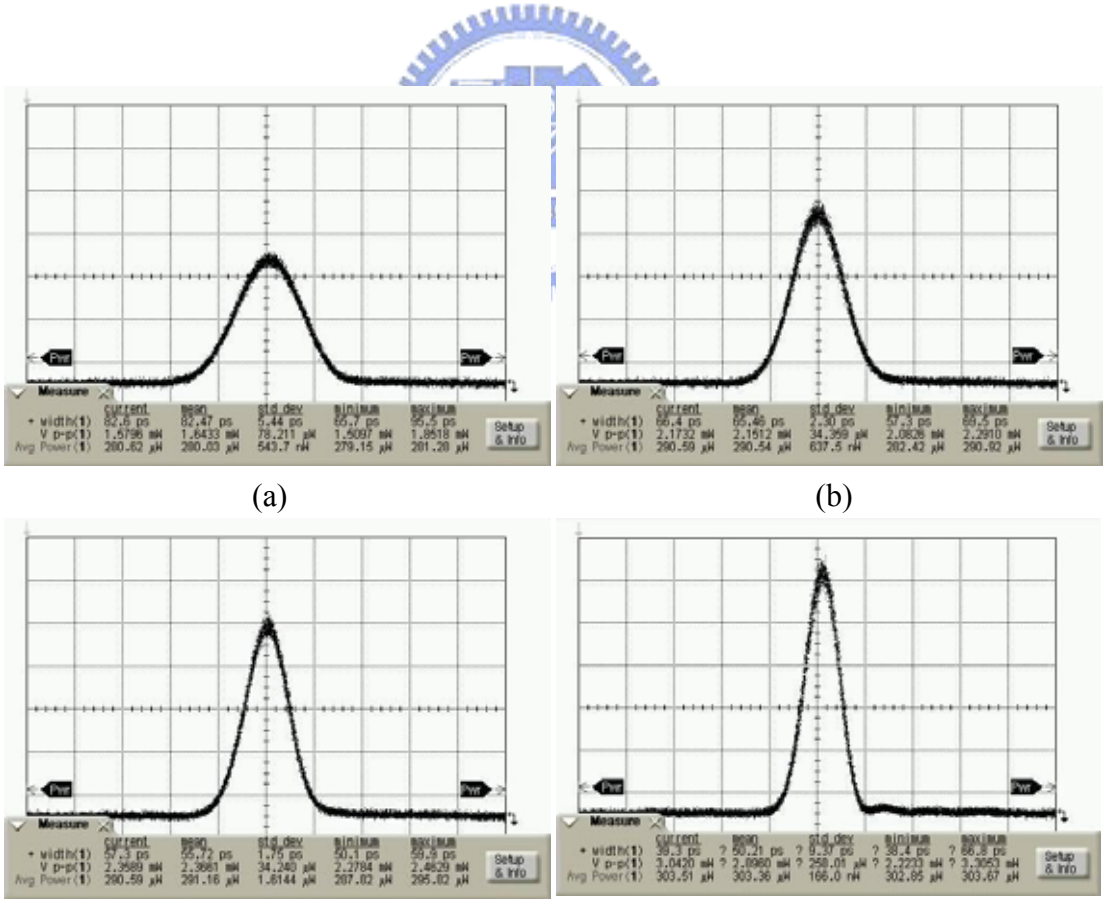

(a) (b)

(c) (d)

Figure 3.10 The pulsewidth is changed by using the polarization controller. Pulsewidth **(a)** 82 ps **(b)** 66ps **(c)** 56ps **(d)** 39ps.

3.2.2 Operating at 10GHz

Operating at 10GHz, most of parameters of the mode-locked laser are the same as that operated at 2GHz repetition rate. Unfortunately, as operating at higher repetition rate, the problem, such as the polarization fluctuations and timing jitter, induced by the fluctuations, for example something like the change of the fiber cavity length induced by thermal, will become more serious than operated at lower repetition rate. As the length changed, it makes the operating modulation frequency not at the n-th harmonic modes of the fundamental repetition rate of the cavity. The laser output will become unstable and blurred. As the experiment showing later, the phenomenon will become more obvious while it is operated at 40 GHz repetition rate. Therefore, the repetition rate operated at 10 GHz was not as stable as operated at 2GHz, especially a length of unavoidable signal mode fiber in the cavity.

As figure 3.11 shown, it is measured by Agilent 86116A in different time window spans. The optical channel unfiltered bandwidth of 86116A is 50GHz, and transition time is 9.0ps (FWHM). The output pulsewidth of the laser is about 22ps, and the optical spectral bandwidth is about 0.167nm shown in figure 3.12. Figure 3.13 shows the waveform measured by autocorrelator. The solid line is Gaussian fitting curve and pulsewidth is measured about 18ps. The time-bandwidth product is 0.459, which means that the output pulses are also approaching transform-limited for Gaussian shape even the repetition rate operated at 10GHz. By using 100mW pumping power, the average output power of the laser is about 0.26mW and peak power is about 1.16mW. The RF spectrum is shown in figure 3.14. The span of the left figure is 20MHz, and another is 100MHz. Using the polarization controller, if the state of polarization was adjusted properly, the supermode suppression ratio (SMSR) can be above 52dB. The parameters of the mode-locked laser operated at 10GHz repetition rate are listed in Table 3.3.

Input parameters	
980nm pump:	100 mW
cavity length:	39 m
mode spacing:	5.12 MHz
repetition rate:	10 GHz (about 2000th harmonic)
modulation strength	17 dBm
Results	
central frequency:	1550 nm
SMSR:	> 52 dB
output average power:	0.26 mW
output peak power:	1.16 mW
optical spectrum bandwidth:	0.167 nm
Pulse width (FWHM):	22 ps
time-bandwidth product:	0.459

Table 3.3 Parameters of the mode-locked laser operated at 10GHz repetition rate

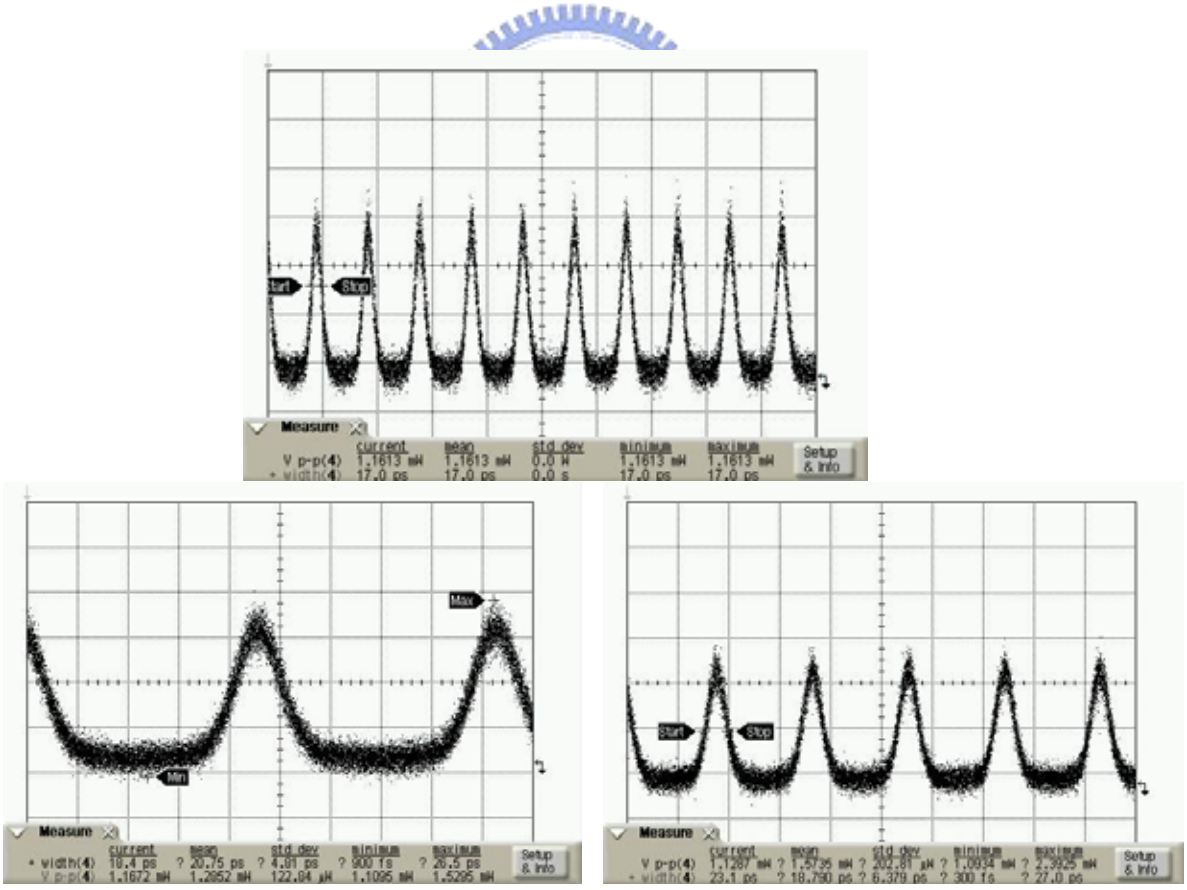

Figure 3.11 The waveform operated at 10GHz is measured by Agilent 86116A in different time window spans.

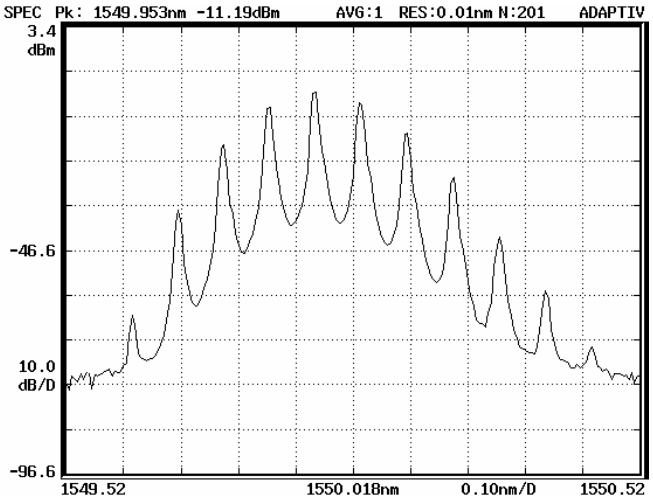

Figure 3.12 Optical spectrum

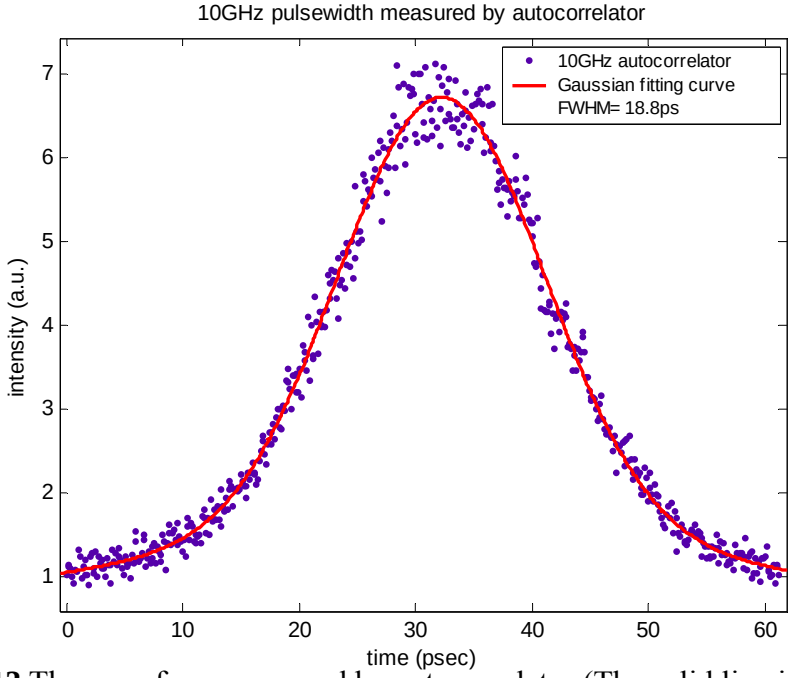

Figure 3.13 The waveform measured by autocorrelator (The solid line is Gaussian fitting curve)

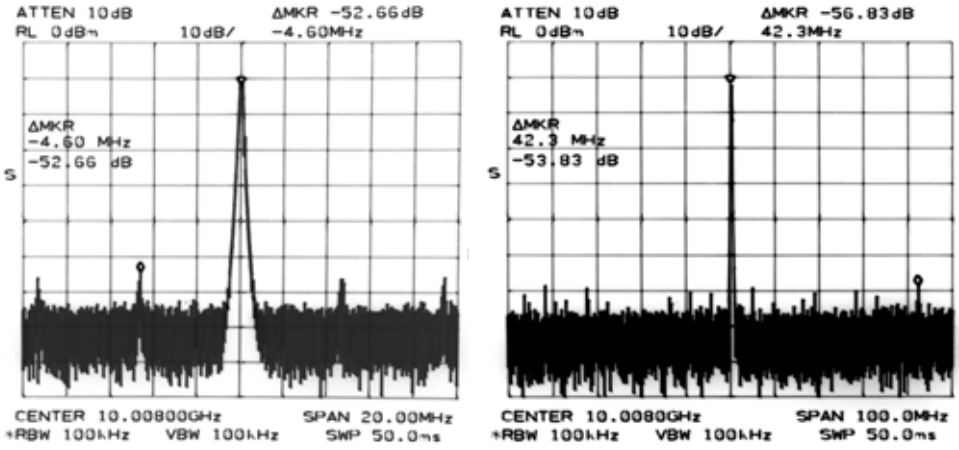

(a) (b)

Figure 3.14 RF spectrum **(a)** span: 20MHz, SMSR: 52dB

(b) span: 100MHz, SMSR: 53dB

3.3 Setup of the experiment (operating at 10GHz, 20GHz and 40GHz)

Figure 3.15 shows the experimental setup. The EO*SPECE* 40GHz modulator was utilized to operating from 10GHz to 40GHz repetition rate in this structure. Fortunately, there are all polarization maintaining (PM) fibers in the cavity and the total length of the laser cavity is shorter than previous structure. Therefore, the outside influences to the stabilization of the laser were not as serious as before. The output of all PM fibers structure even without the polarization controller is still conspicuously stable. Because there is no unavoidable effect on the polarization state of cavity, for example a length of SMF, a polarization controller is not necessary anymore.

Unfortunately, the optical tunable filter which was used previously made the polarization state unstable in all PM fiber cavity so that the output pulse train became blurred and unstable while the optical filter was put into the cavity. Besides, the filter also limits the spectral bandwidth of the pulse. It means that the pulsewidth is also relatively limited by the filter bandwidth. The 3dB bandwidth of our filter is 0.582nm at 1550nm. Therefore, it is not used here.

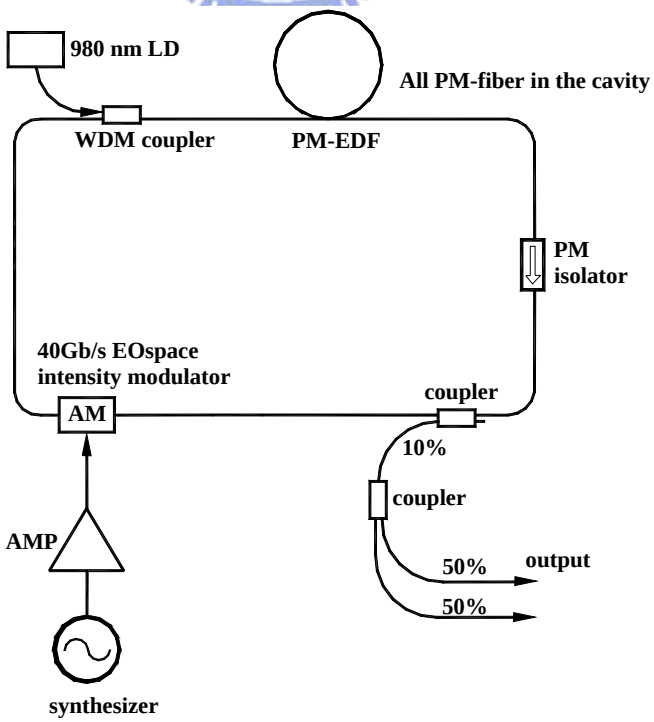

Figure 3.15 The experimental setup

3.3.1 Operating at 10GHz

The total cavity length is about 32m and its' fundamental repetition rate is about 6.25MHz. Comparing with previous laser using JDSU modulator operated at 10GHz, this active mode-locked fiber laser with all PM fiber is much more stable and has shorter pulsewidth as shown in figure 3.16. It is measured by Agilent 86116A in different time window spans. By using the Agilent precision time base 86107A, the time base linearity error is smaller than 100 femto-seconds. The measuring pulsewidth of the laser is about 13ps and the optical spectral bandwidth is about 0.375nm shown in figure 3.17. Figure 3.18 shows the waveform measured by autocorrelator. The solid line is Gaussian fitting curve and pulsewidth is measured about 11.07ps. The time-bandwidth product is small than 0.51. With 100mW pumping power, the average output power of the laser is about 0.93mW and peak power is about 5.7mW. The RF spectrum is shown in figure 3.19 and the span of the spectrum is 100MHz. The supermode suppression ratio (SMSR) is about 53.6dB. The parameters of the mode-locked laser at 10GHz repetition rate are listed in Table 3.4.

Input parameters	
980nm pump:	100 mW
cavity length:	32 m
mode spacing:	6.25 MHz
repetition rate:	10 GHz (about 1600th harmonic)
modulation strength	17.5dBm
Results	
central frequency:	1563 nm
SMSR:	53 dB
output average power:	0.93 mW
output peak power:	5.7 mW
optical spectrum bandwidth:	0.375 nm
Pulse width (FWHM):	11.07 ps (measured by autocorrelator)
time-bandwidth product:	0.51

Table 3.4 Parameters of the mode-locked laser operated at 10GHz repetition rate

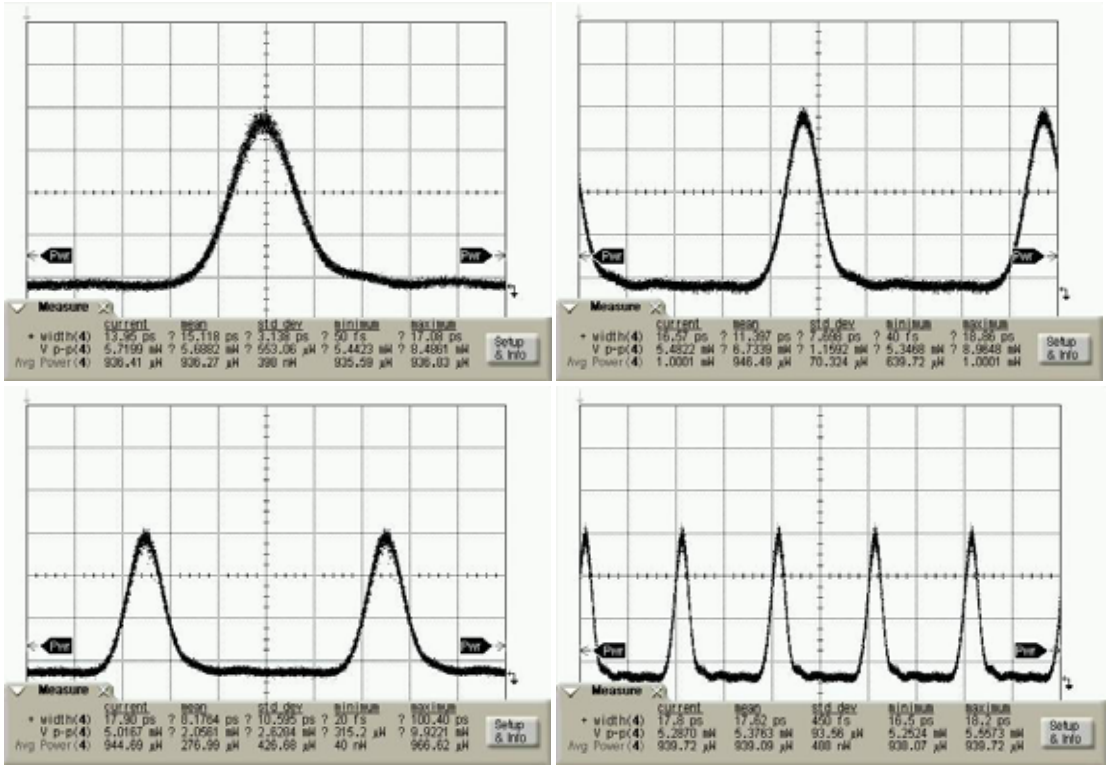

Figure 3.16 the pulse train operated at 10GHz is measured by Agilent 86116A in different time window spans.

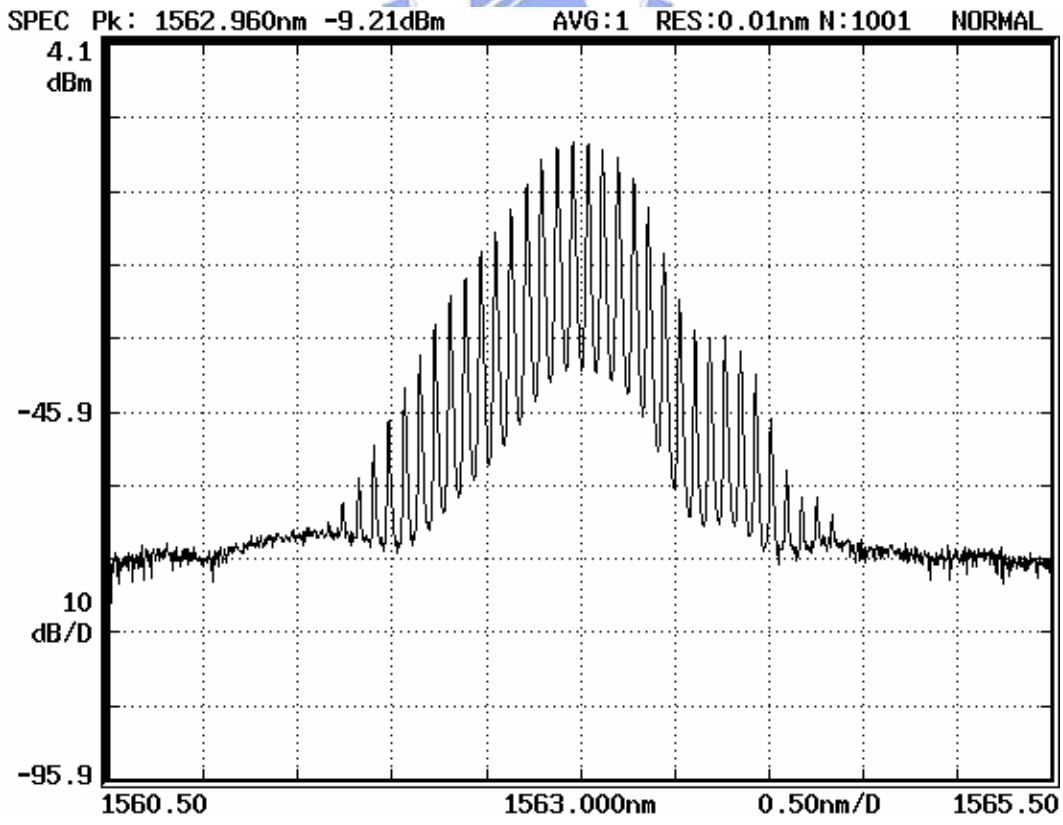

Figure 3.17 Optical spectrum

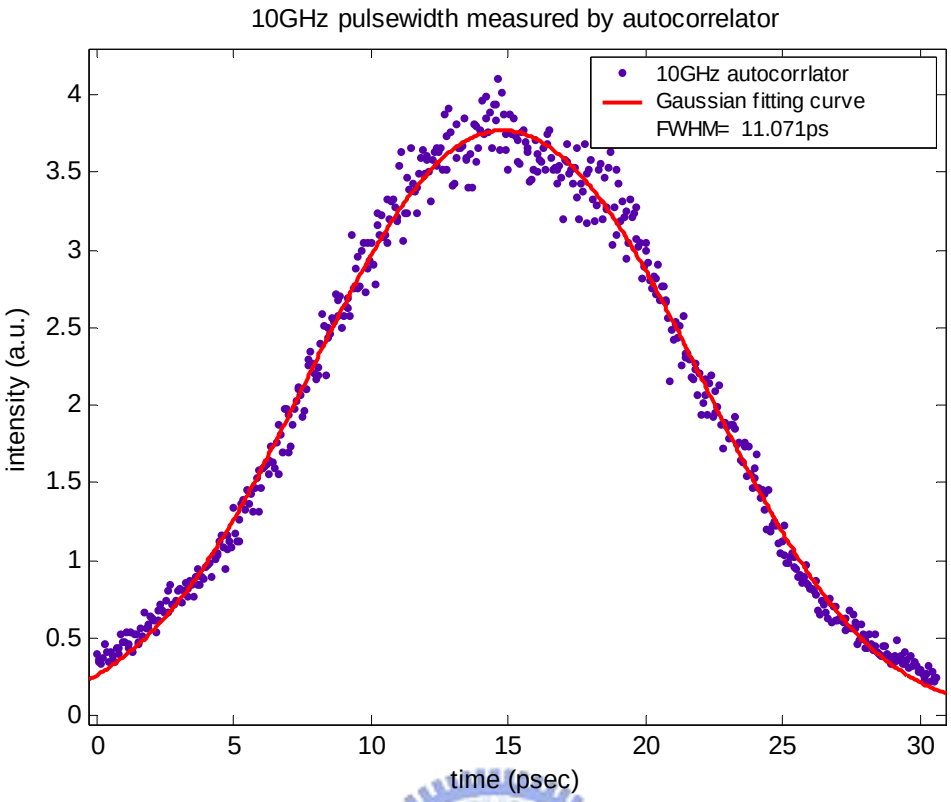

Figure 3.18 the waveform measured by autocorrelator (The solid line is Gaussian fitting curve)

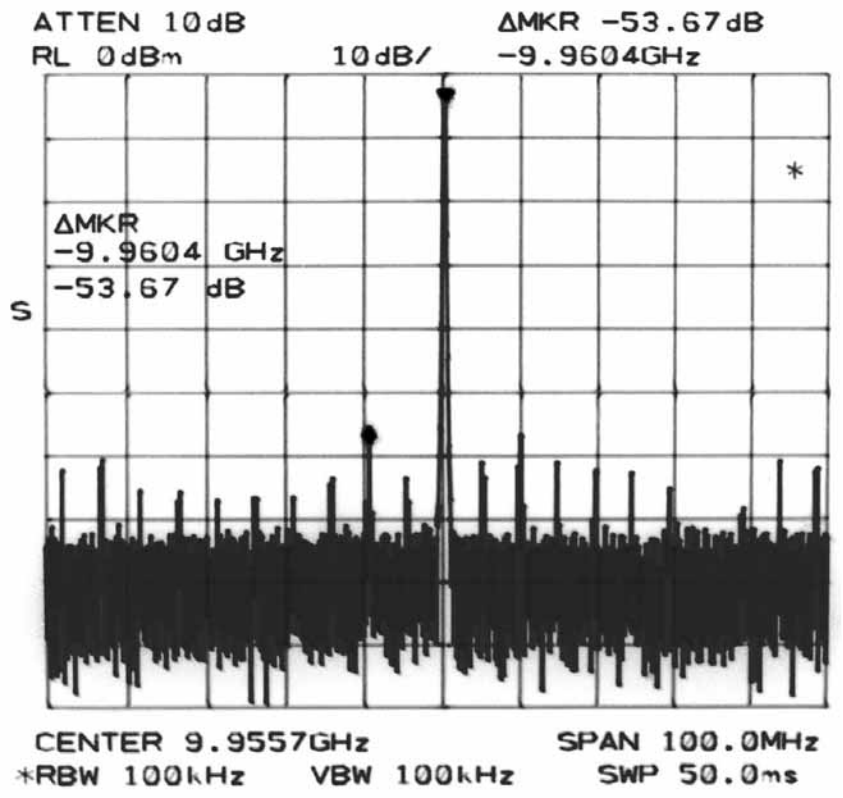

Figure 3.19 RF spectrum, span: 100MHz, SMSR: 53 dB

3.3.2 Operating at 20GHz

Operating at 20GHz repetition rate, most of parameters of the mode-locked laser are as same as that operated at 10GHz repetition rate at the subsection 3.3.1. Figure 3.20 shows the laser output waveform measured by Aglient 86116A. In figures, these obviously little ripples are because of the limited bandwidth of the sampling oscilloscope (86116A). It can be proven by using the autocorrelator to measure it which is shown in figure 3.21.

Figure 3.22 shows the waveform measured by autocorrelator. The solid line is Gaussian fitting curve and pulsewidth is about 7.81ps. The optical channel unfiltered bandwidth of 86116A is 50 GHz, and transition time is 9.0ps (FWHM). Therefore, this pulsewidth have exceeded the minimum pulsewidth which can be measured by Agilent 86116A. This phenomenon will be more obviously while measuring the pulsewidth as short as 40GHz pulse train. Although the bandwidth of the instrument is not enough to display and measure the real waveform and pulsewidth, the information of the out pulse is clean or blurred still can be clearly displayed by the sampling oscilloscope.

The optical spectral bandwidth of the output pulse is about 0.48nm shown in figure 3.23. The time-bandwidth product is about 0.461, which means that the output pulses of the fiber laser operated at 20GHz repetition rate are still approaching transform-limited for Gaussian shape. By using 100mW pumping power, the average output power of the laser is about 0.9mW and peak power is about 3.5mW. The RF spectrum is shown in figure 3.24 and the span is 50MHz. The supermode suppression ratio (SMSR) is still above 50dB. The parameters of the mode-locked laser operated at 20GHz repetition rate are listed in Table 3.5.

Input parameters	
980nm pump:	100 mW
cavity length:	32 m
mode spacing:	6.25 MHz
repetition rate:	20 GHz (about 3200th harmonic)
modulation strength	15.5dBm
Results	
central frequency:	1563 nm
SMSR:	56 dB
output average power:	0.9 mW
output peak power:	5.7 mW
optical spectrum bandwidth:	0.48 nm
Pulse width (FWHM):	7.81 ps (measured by autocorrelator)
time-bandwidth product:	0.461

Table 3.5 Parameters of the mode-locked laser operated at 20GHz repetition rate

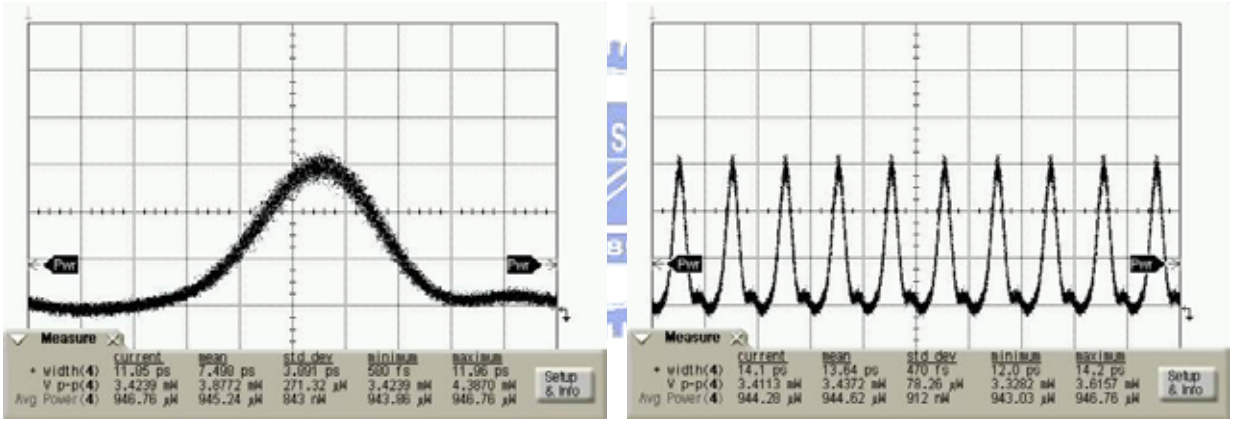

Figure 3.20 The waveform operated at 20GHz is measured by Agilent 86116A in different time window spans.

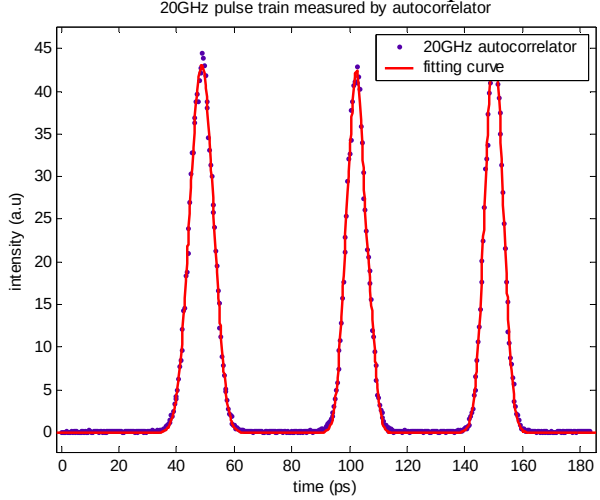

Figure 3.21 The 20GHz pulse train measured by autocorrelator (The solid line is Gaussian fitting curve)

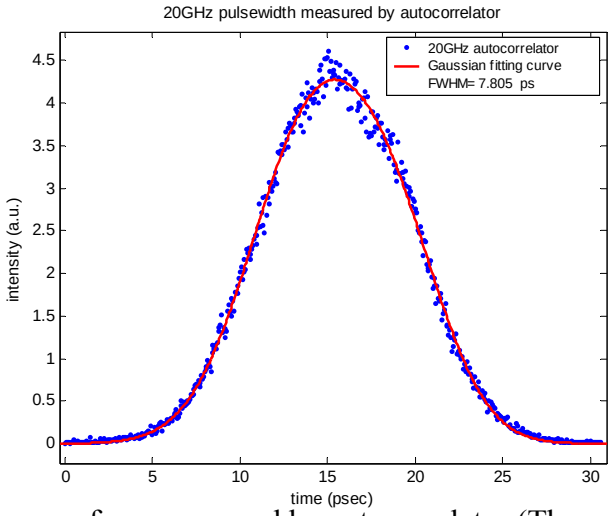

Figure 3.22 The waveform measured by autocorrelator (The solid line is Gaussian fitting curve)

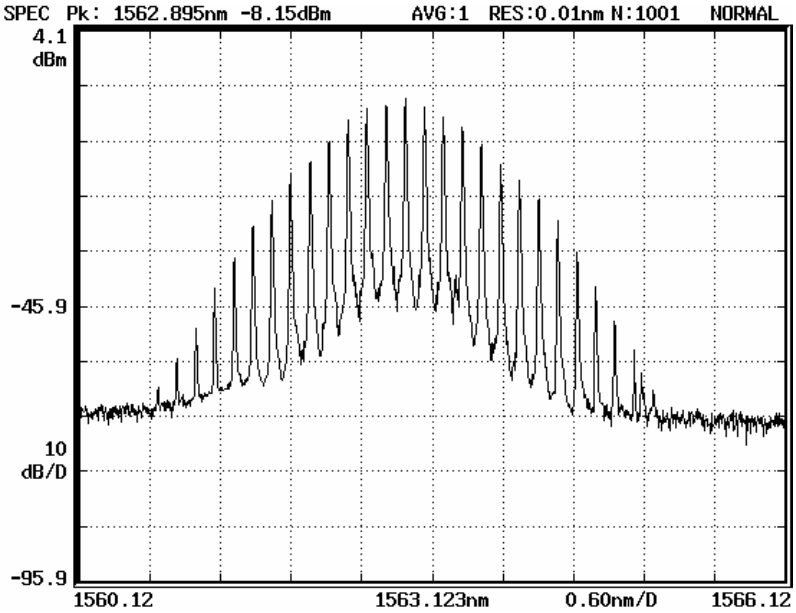

Figure 3.23 Optical spectrum

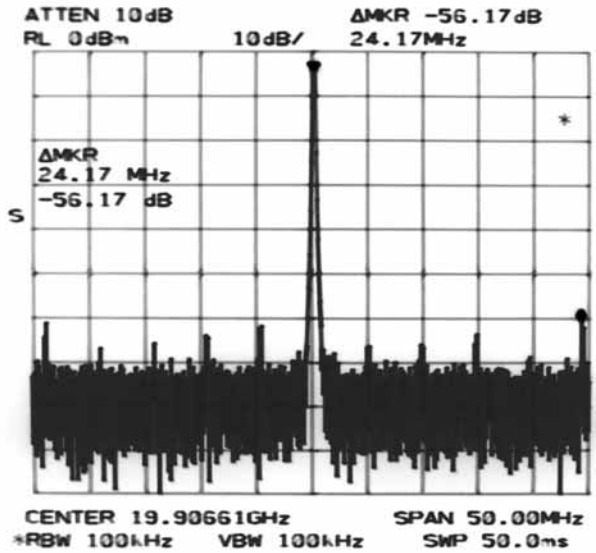

Figure 3.24 RF spectrum, span: 50MHz, SMSR: 56 dB

3.3.3 Operating at 40GHz

The response of RF amplifier operated at 40GHz is not as good as operating at 10GHz or 20GHz. Although the modulation strength is only about 10dBm, 40GHz mode-locked fiber laser have been successfully achieved here. Figure 3.25 shows the waveform measured by Agilent 86116A. According to equation (2.2.10), it is known that the pulsewidth will become narrower while the laser operated at higher repetition rate. The pulsewidth of the laser operated at 40GHz is about 3.31ps measured by autocorrelator as shown in figure 3.26. Even if the bandwidth of sampling oscilloscope of Agilent 86116A is not larger enough to display the real information of the waveform and pulsewidth, the information that the pulse is clean can still be obtained from figure 3.26. By using the autocorrelator, the figure 3.27 shows the real pulse train of the laser. But, unfortunately, operating at as high as 40GHz repetition rate, while a small perturbation such as a mechanical vibration or thermal expansion is applied to the cavity, the absolute frequency compared with that in ordinary lasers will change. It means that if the matching between the cavity mode separation frequencies from the synthesizer is lost, the phase between the modes is not locked and eventually instability occurs as shown in the figure 3.28. In reality, it is difficult to maintain the optimum operational conditions over a long time, though it is possible to generate clean short pulses in a short time.

The optical spectral bandwidth of the output pulses is about 1.2nm shown in figure 3.29. The time-bandwidth product is about 0.488, which means that the output pulses also approaches transform-limited for Gaussian shape even the repetition rate operated at 40GHz. With 110mW pumping power, the average output power of the laser is about 1.0mW and peak power is about 3.5mW. At the steady state, depending on the experience, above 50dB SMSR is still available here. The parameters of the mode-locked laser operated at 40GHz repetition rate are listed in Table 3.6.

Input parameters	
980nm pump:	110 mW
cavity length:	32 m
mode spacing:	6.25 MHz
repetition rate:	40 GHz (about 6400th harmonic)
modulation strength	10 dBm
Results	
central frequency:	1562 nm
output average power:	1.0 mW
output peak power:	3.5 mW
optical spectrum bandwidth:	1.2 nm
Pulse width (FWHM):	3.308 ps (measured by autocorrelator)
time-bandwidth product:	0.488

Table 3.6 Parameters of the mode-locked laser operated at 40GHz repetition rate

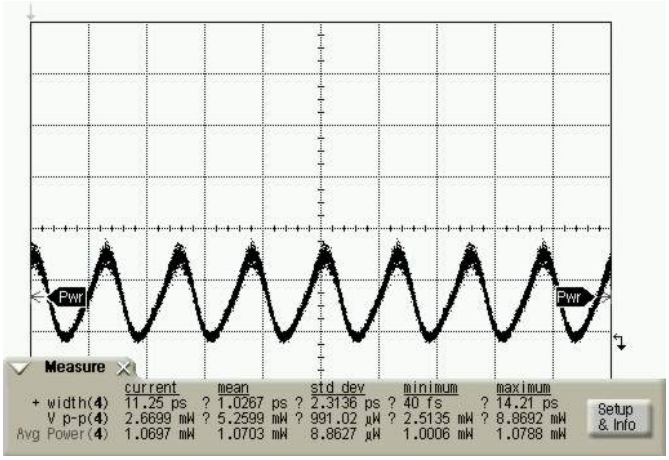

Figure 3.25 The waveform operated at 40GHz is measured by Agilent 86116A in different time window spans.

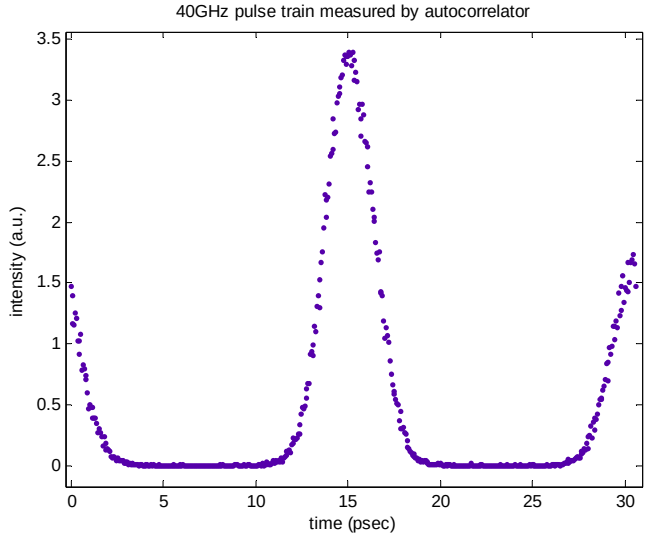

Figure 3.26 the 40GHz pulse train measured by autocorrelator

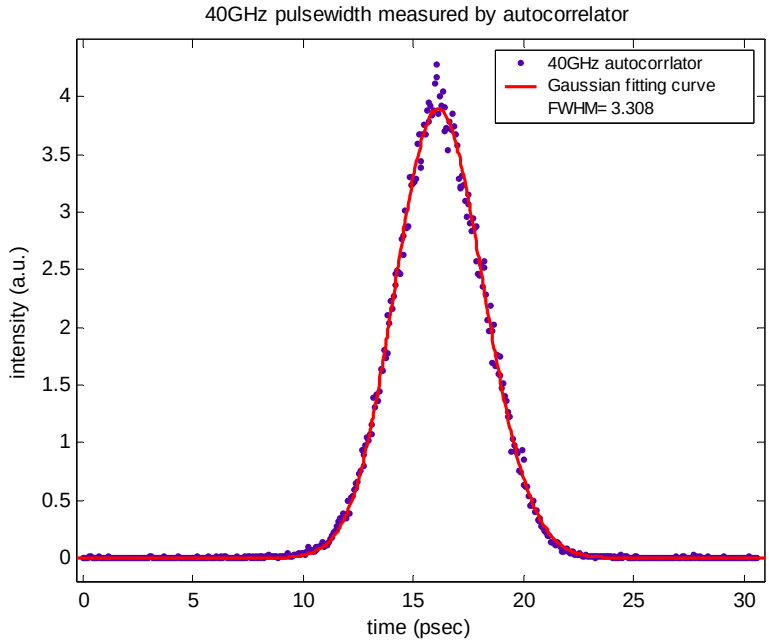

Figure 3.27 The waveform measured by autocorrelator (The solid line is Gaussian fitting curve)

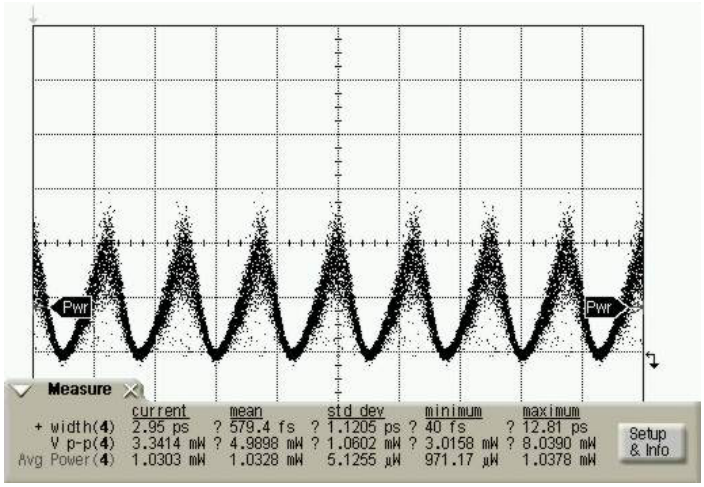

Figure 3.28 Because of some perturbations, the phase between the modes is not locked and eventually instability occurs.

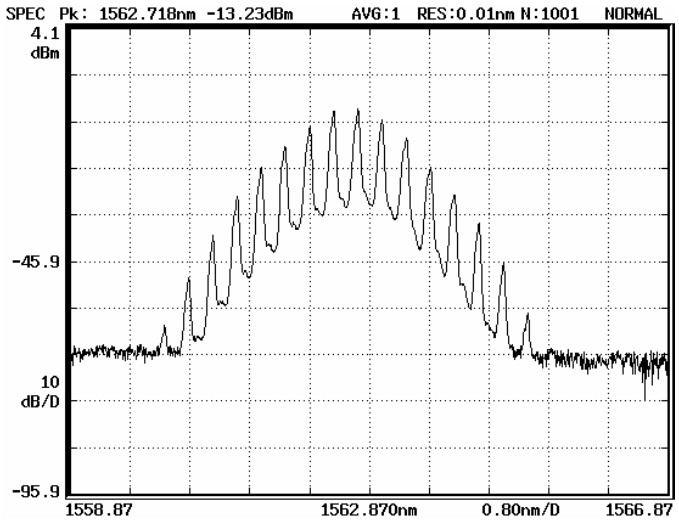

Figure 3.29 Optical spectrum

CHAPTER 4

Simulations

4.1 Introduction of VPI

Simulation of photonic systems has become a necessity due to the complex interactions within and between components. However, simulation does have some intrinsic disadvantages over laboratory prototypes: an ultra high speed system prototype will always be able to generate information at a greater rate than the fastest computer. On the other hand, simulation has advantages, for one, parameters can be set and adjusted with far more certainty than in reality, and measurement errors can be eliminated by removing reflections, unknown losses, and even noise in some cases. Any design process using novel components should include laboratory prototypes, at least until the simulation is verified for these components.

Otherwise, component interactions are complex, and can be highly nonlinear in nature. For this reason alone, computer simulation has become an essential part of the design process of optical fiber system. VPI includes the ability to capture the physics of components' behavior in numerical models in such a way that the effects of interactions of components can be predicted, for almost any topology.

The simulation tools of VPI is graphical user interfaces (GUIs). GUI became a necessity as simulation tasks moved outside the boundaries of a single device. This is because the topology of the "photonic circuit" becomes as important as the components themselves. A GUI enables complex topologies to be assembled quickly and with visual error checking. Moreover, GUIs have also been used extensively for device simulation, where two- and three-dimensional problems are naturally candidates for graphical entry.

This simulation tools are used for many layers of telecommunications network design, from demand forecasting, service provisioning, and transport network optimization, through equipment, component and device design, to the details of material design.

By using the VPI, to simulate the rapid bidirectional interactions between components, data was passed between the component models sample-by-sample. It is called “Sample Mode”. As shown in figure 4.1, there is a two-stage iteration process: first, all models are run to calculate their internal states, such as optical fields; second, data is exchanged between adjacent modules to be used to build up the waveform at the output of the circuit. Thus, all components have to be active throughout the simulation.

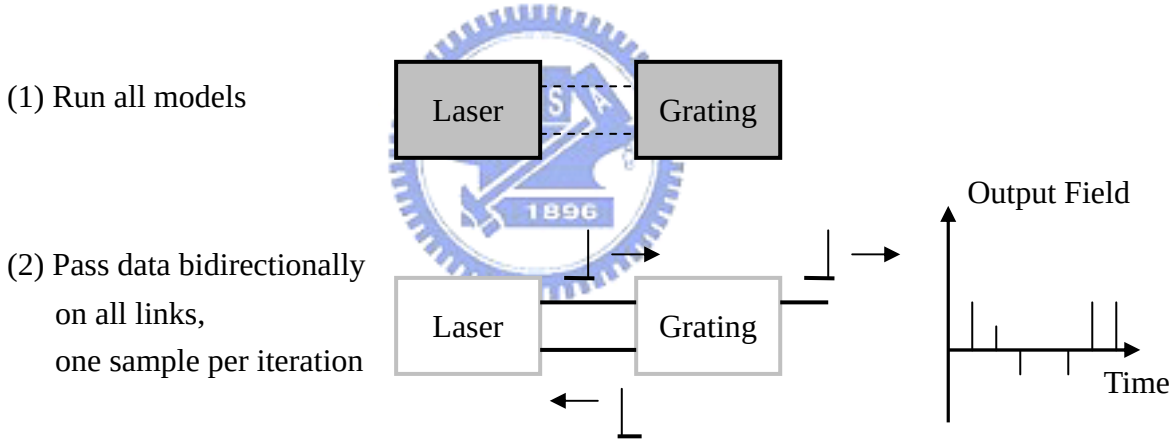

Figure 4.1 Bidirectional simulation algorithms. Step1 and 2 are repeated to build up a waveform [31].

In “Black Mode”, it is operated by passing blocks of data in a “forward” direction. As shown in figure 4.2, first, the signal source (usually the data generator or transmitter) is run first; this generates a block of data representing a signal waveform or its spectrum; second, the block of data is then passed to the next module, such as the fiber; third, the next module is then run to proves the data and so on, until the receiver or instrumentation is reached.

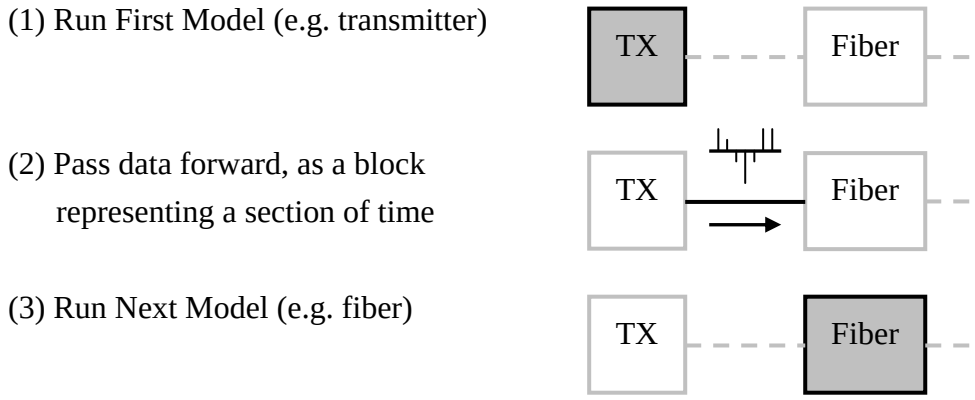

Figure 4.2 Passing data unidirectional simplifies calculations and slows data to be processed efficiently in blocks [31].

VPI allows models of devices, components, and subsystems to be chosen and wired together. The scheduler of a simulator sets the execution order of the modules to ensure each module has appropriate input data before execution. They set photonic simulators apart in their libraries of photonic components, into which a great deal of design and implementation effort is put.

Besides, a model of a component in a simulator contains a large amount of intellectual property. During its development, many details have to be considered and techniques developed. This is illustrated in figure 4.3. First, a decision to create a model has to be made based on a thorough knowledge of current and likely simulation tasks and component developments. The model parameters then have to be decided upon and defined unambiguously with due consideration to the level of abstraction of the model. The physics of the device then has to be considered before appropriate numerical algorithms are developed. The algorithms must solve the problem efficiently and consider all types of signals that are to be processed. The complete specification of the model must then be implemented and tested, including real-word comparisons. Topical application examples are then developed to help users understand and apply the models most efficiently. The module and its applications

must be thoroughly documented, and training examples developed. Finally, a database of support questions and answers will evolve, and this can be used to define future developments to the model.

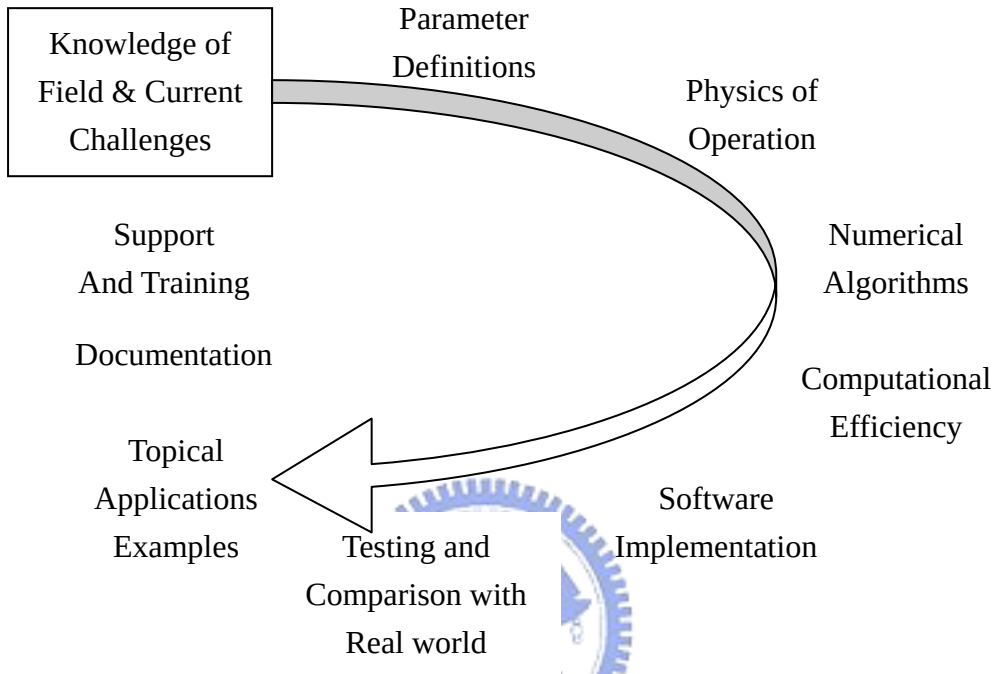

Figure 4.3 Considerations when developing a model [31]

VPI is very mighty simulation tool. This introduction cannot include the details of the physical understanding and numerical techniques. More details can be available from reference book [31].

In order to ensuring the accuracy of the simulation, the simulation whose experiment has been reported in national journal was simulated first in the next subsection 4.2. In section 4.3, the experimental setup in chapter 3 was simulated and simulation results were compared with the experimental results, such as pulsewidth, optical spectrum, and time-bandwidth product.

4.2 Simulations

In this subsection, in order to make sure that the simulation is correct, it must be confirmed by comparing with acknowledged experimental results. Figure 4.4 shows the experimental structure of harmonic mode-locked fiber laser and it has been reported in Electronics Letters in 1994 [30]. The authors reported the operation of a harmonically and regeneratively mode-locked fiber ring laser at 1550nm. By incorporating a soliton narrowing effect in the cavity, pulse train with a 2.7~5ps pulsewidth was obtained at a 10GHz repetition rate.

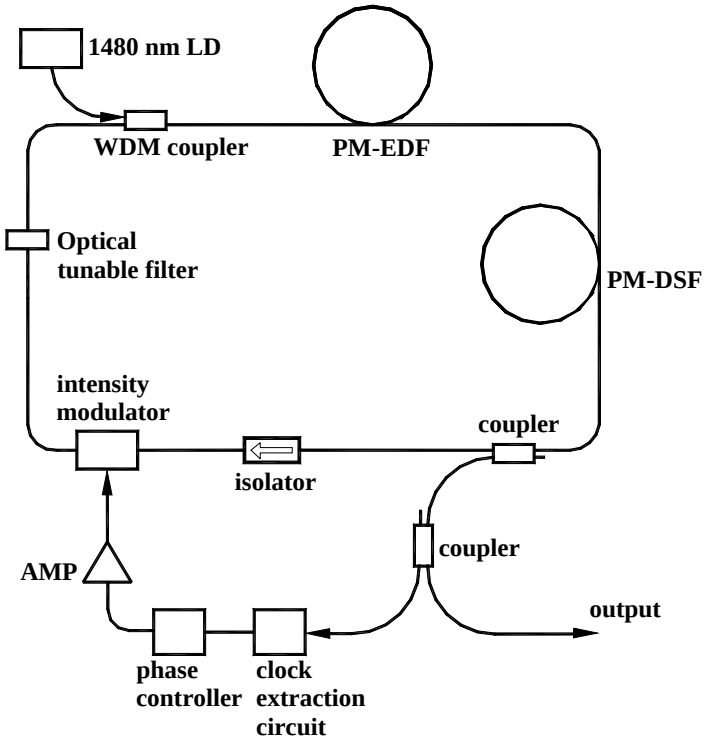

Figure 4.4 The experiment structure [30].

The laser has a unidirectional ring cavity constructed with a 15m polarization maintaining erbium-doped fiber (PM-EDF), a WDM coupler for pumping the erbium-doped fiber (EDF) with 1480nm laser diodes, about 200m polarization maintaining dispersion shifted fiber (PM-DSF 3.4ps/km/nm) for soliton compression, a 15% output coupler, a polarization-dependent isolator, an $LiNbO_3$ modulator, and an optical filter with bandwidth of 2.5nm.

Without the PM-DSF, the output pulsewidth was 7.0ps and it can be shortened to as short as 2.7ps through the use of the soliton effect by using PM-DSF for dispersion management in the cavity. The optical spectral is shown in figure 4.5 (a). The spectral bandwidth for a 2.7ps output pulsewidth is 1.0nm, resulting in a time-bandwidth product of 0.34. The changes in pulsewidth and output power with and without the soliton effect are shown in figure 4.5 (b) against pumping power. Without the soliton effect, the PM-DSF is not installed in the cavity, the output pulsewidth was 7ps. No change in the pulsewidth was observed when the pump power was varied, while the output power increased linearly. Comparatively, when the soliton effect using PM-DSF is incorporated, the output pulsewidth is shortened with increasing in the pumping power.

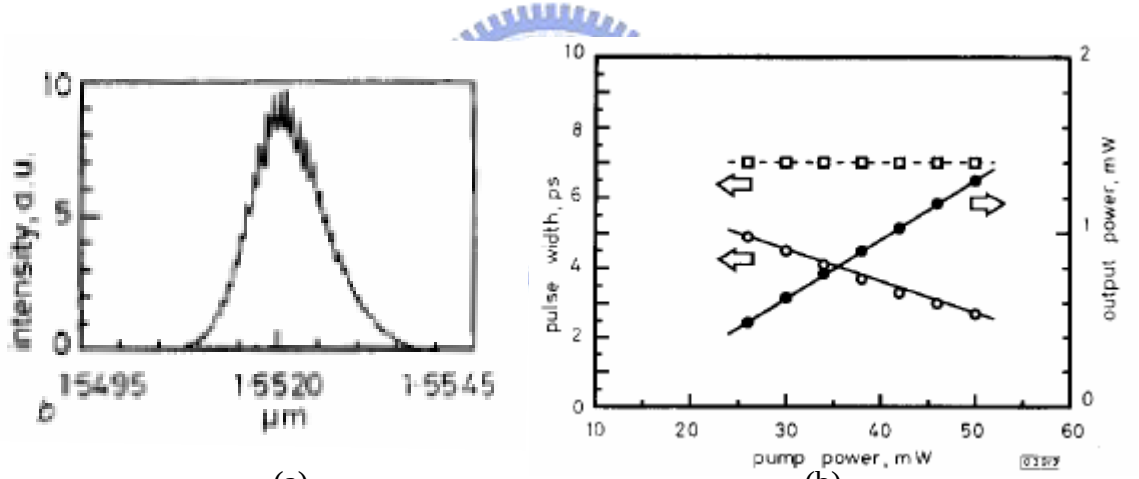

(a) (b)

Figure 4.5 (a) optical spectrum (b) Changes in pulsewidth and output power against pumping power [30]

In this work, if the simulation model is required to come closer to reality, the parameters and the data flow of simulation will become more complex and larger. Beside, in order to get accurate results, thousands of iteration is necessary for laser model using the VPI. Thus, it took a lot of time, maybe few days. Therefore, the representative results are selected to represent here. By using VPI, the simulation

structure is the same with figure 4.4. Without PM-DSF, the pulsewidth of the simulation is about 7.15ps. The waveform is shown in figure 4.6. With PM-DSF, the pulsewidth is as short as 3.02ps shown in figure 4.7. The optical spectrum of 3.02ps pulsewidth is shown in figure 4.8 and the bandwidth is about 0.89nm. The time-bandwidth product is 0.335. The comparison with the experiment results is listed in Table 4.1.

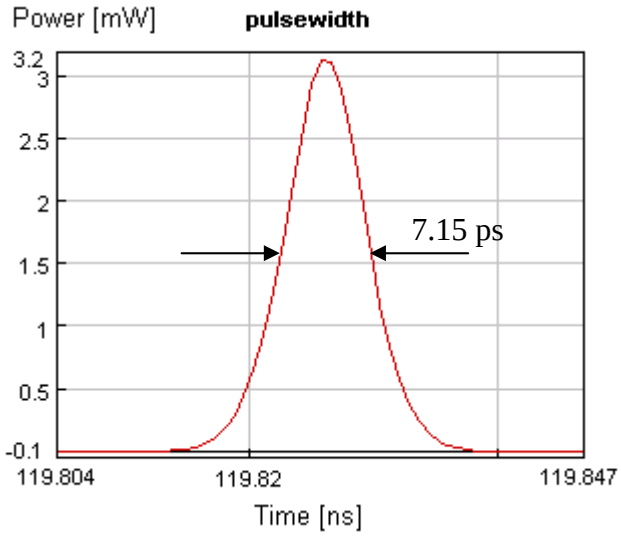

Figure 4.6 Waveform of simulating output pulse train without dispersion shift fiber (Full Width Half Maximum (FWHM): 7.15ps)

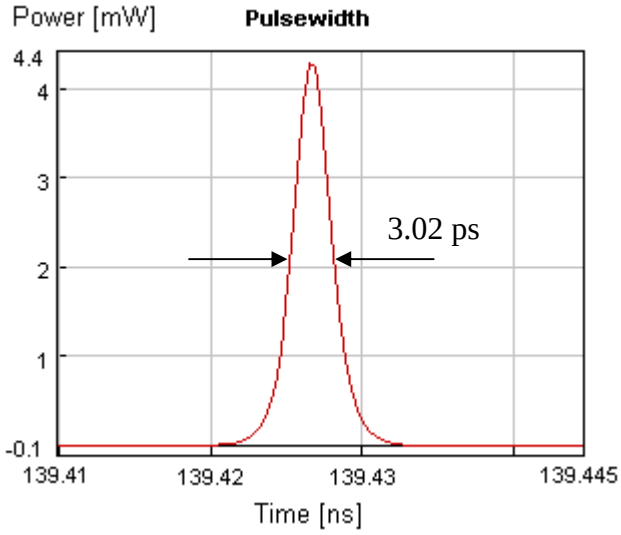

Figure 4.7 Waveform of simulating output pulse train with dispersion shift fiber (FWHM: 3.02ps)

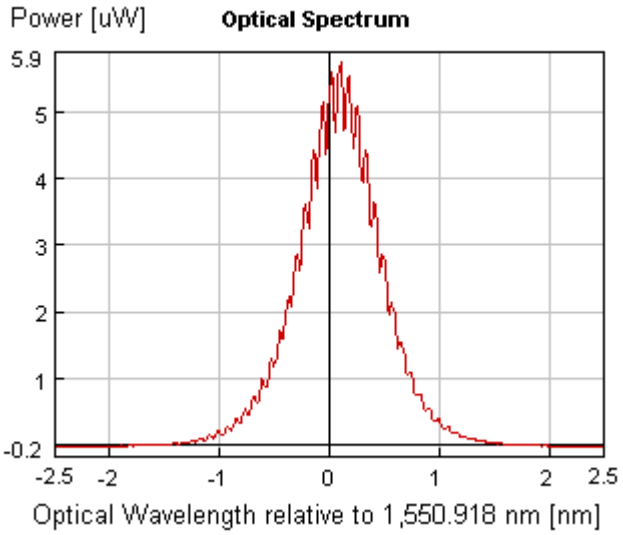

Figure 4.8 Optical spectrum of 3.02ps pulsewidth

	Simulation results	**experiment**
Pulsewidth (w/o DSF)	7.15 ps	7.00 ps
Pulsewidth (with DSF)	3.02 ps	2.70 ~ 5.00 ps
$\Delta f \cdot \Delta \tau$ **(with DSF)**	0.335	0.340

Table 4.1 Comparison between simulation and experimental result.

Consequently, comparing simulation results with experimental results which have been reported in national paper, the simulation is very close to experiment. Therefore, by using VPI, the simulation of active mode-locked erbium-doped fiber laser and its result is reliable here. In the next section, our experimental structure in chapter 3 will be simulated and compared with the real results.

4.3 Experimental simulation

The simulation setup is shown in figure 4.9. The continue wavelength laser, which is displayed as “LaserCW”, is just used to define the simulation frequency range through WDM coupler. Its power is negligible. Forward pumping was utilized here through the WDM coupler pumping into cavity and the pumping power is about 50mW. One of advantages of simulations is that the considerations of environment perturbations, such as a mechanical vibration or thermal expansion, do not take place here. The detail of the simulation component is listed in table 4.2 [32]. All the simulation components are setting polarization-maintaining. Our cavity is made up of “AmpEDFA”, “Attenuator”, “FilterGaussBP”, “FiberNLS”, and “ModulatorMZ” etc la. The bandwidth of optical filter is 72.5 GHz (~0.582nm). After through the module of fiber, “Fork” plays as a coupler and separates the data flow. The Mach-Zehnder modulator was driven by “FuncSineB” which plays as a RF synthesizer in reality. After passing through the “Fork”, output pulse train of simulating active mode-locked fiber laser and the results of pulsewidth were measured by “ViScope”. The optical spectrum was displayed by “ViOSA”.

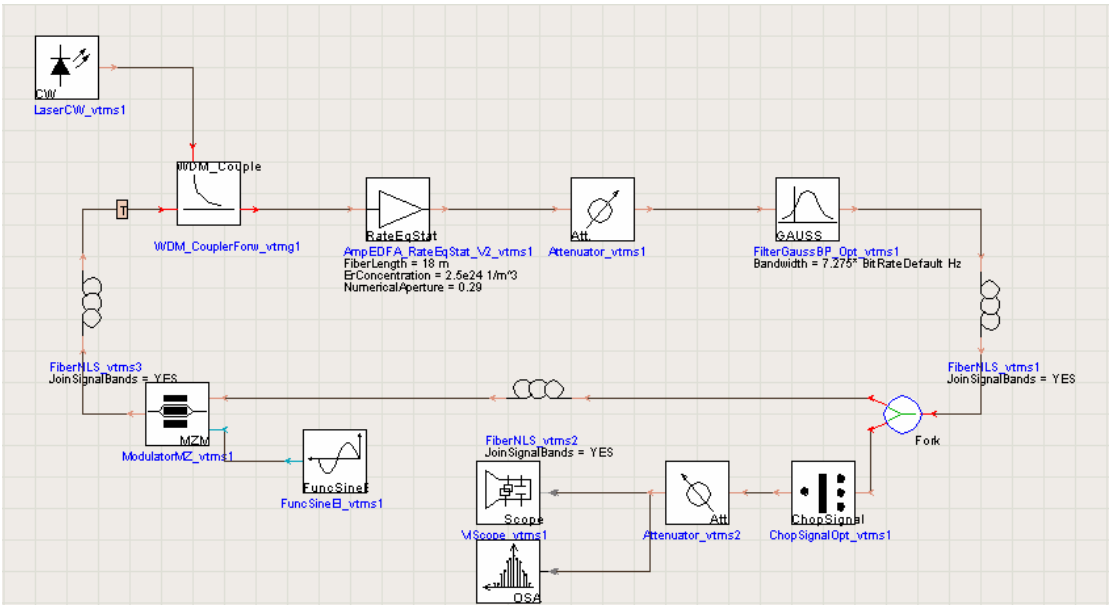

Figure 4.9 The simulation structure of VPI

Component name	Characteristic
Laser CW (continuous wavelength laser)	Generates a continuous wave (cw) optical signal of a DFB laser
WDM_coupler	This module represents a signal-pump multiplexer for a forward-pumped doped fiber amplifier. The signal and pump multiplexing losses can be controlled individually.
AmpEDFA (erbium doped fiber)	This module simulates an erbium-doped fiber amplifier (EDFA) subsystem. The EDFA subsystem includes forward and backward pump sources, and optional pump reflecting and polarization filters.(rate- and propagation equation model)
Attenuator	Optical Attenuator
FilterGaussBP (optical tunable filter)	The module simulates an optical filter with a Gaussian-shaped band-pass transfer characteristic. The filter is dispersion less.
FiberNLS (fiber)	Nonlinear Dispersive Fiber (NLS), model solves the non-linear Schroedinger equation. This model takes into account stimulated Raman scattering (SRS), four-wave mixing (FWM), self-phase modulation (SPM), cross-phase modulation (XPM), first order group-velocity dispersion (GVD), second order GVD, and attenuation of the fiber.
Fork (coupler)	Divides data into two identical paths. Often required for correct scheduling.
ChopSignalOpt	The module accepts multiple blocks and outputs one block per n input blocks. It can be used to discard data such as transients occurring during the search for a steady-state solution.
ViOSA (Optical Spectrum Analyzer)	This module is an optical spectrum analyzer (OSA), however it has much better performance than a grating-based optical spectrum analyzer as its resolution is far superior (equal to the inverse of the global parameter “TimeWindow”). The resolution can be reduced to mimic grating-based optical spectrum analyzers.

Table 4.2 (a) The detailed characteristic of components using in VPI simulation [32]

Component name	Characteristic
ViScope (Sampling Oscilloscope)	This module displays electrical and optical signal waveforms (in the time domain).
FuncSineB (Synthesizer)	This module generates an electrical sine waveform superimposed on a constant bias.
ModulatorMZ (intensity modulator)	This module simulates a Mach-Zehnder modulator and can take into account a frequency chirp resulting from the modulator asymmetry. The module is designed for ease of use, rather than flexibility.

Table 4.2 (b) The detailed characteristic of components using in VPI simulation [32]

4.3.1 Simulation results of 2GHz

By using VPI to simulate 2GHz active mode-locked erbium-doped fiber ring laser (AML-EFRL), figure 4.10 shows the waveform of the output pulse train. The pulsewidth is about 47.03ps. In order to make the simulation more close to the reality, the resolution of optical spectrum analyzer in simulation was set 0.01nm which is the same as the used real one. The optical spectrum of simulation result is shown as figure 4.11, and the right one is the experimental result of 2GHz AML-EFRL. The bandwidth is about 0.076nm and time-bandwidth product is 0.447. Table 4.3 compares the results of simulation with the experiment.

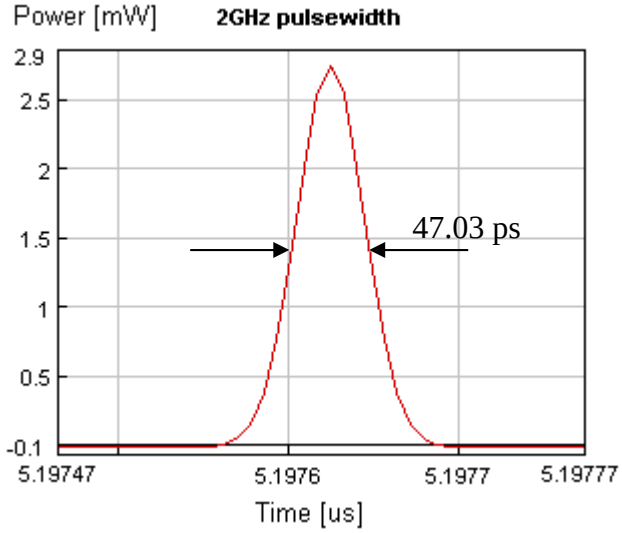

Figure 4.10 Waveform of AML-EFRL operated at 2GHz. (FWHM: 47.03ps)

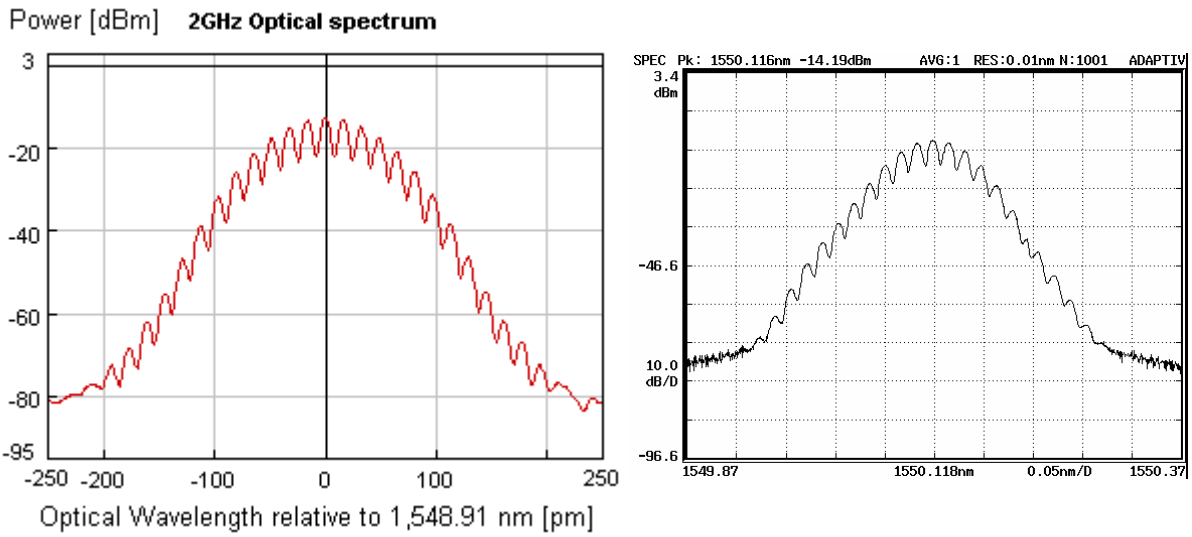

Figure 4.11 Optical spectrum; the simulation result is shown in the left figure and the right one is the experimental result.

	Simulation	Experiment result
Pulsewidth (ps)	47.03	52.00
Bandwidth (nm)	0.076	0.066
Time bandwidth product	0.447	0.429

Table 4.3 Comparing the results of simulation with that of experiment.

4.3.2 Simulation results of 10GHz

Here, two experimental results, cavity with and without optical tunable band pass filter (OTF), are compared. With the "FilterGaussBP", OTF, the structure of the simulation is the same as that operated at 2GHz before. Figure 4.12 shows the waveform of the output pulse train. The pulsewidth is about 20.55ps. The resolution of optical spectrum analyzer in simulation was set 0.01nm. The optical spectrum of simulation result is shown as figure 4.12, and the right one is the experimental result of 10GHz AML-EFRL. The bandwidth is about 0.174nm and time-bandwidth product is 0.447. Table 4.4 compares the results of simulation with the experiment.

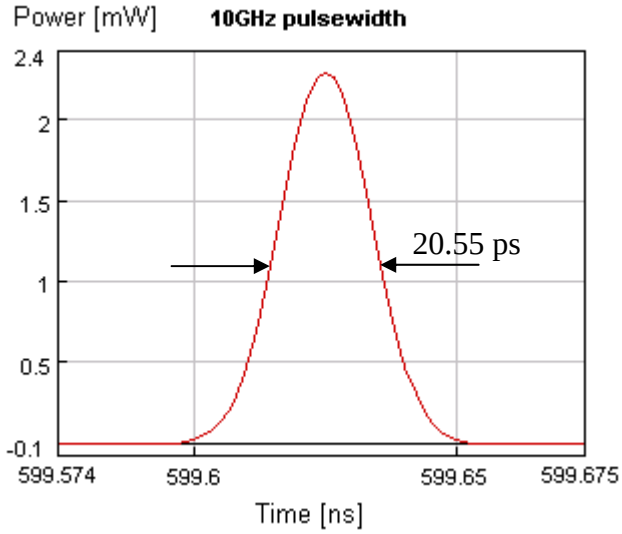

Figure 4.12 Waveform of AML-EFRL operated at 10GHz. (FWHM: 20.55ps)

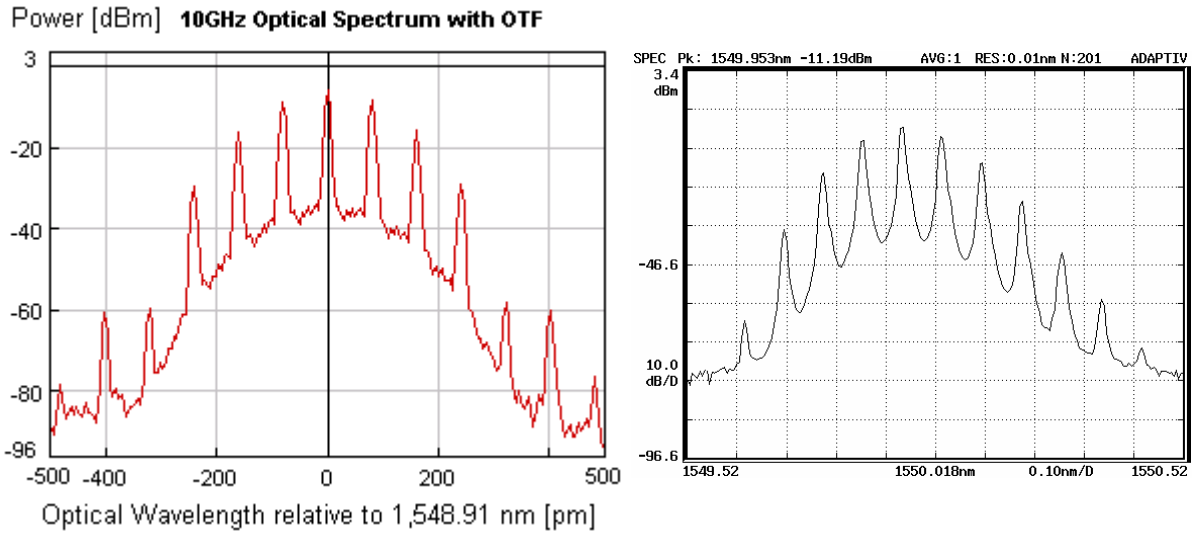

Figure 4.13 Optical spectrum; the simulation result is shown in the left figure and the right one is the experimental result.

	Simulation	**Experiment result**
Pulsewidth (ps)	20.55	22.04
Bandwidth (nm)	0.174	0.167
Time bandwidth product	0.447	0.459

Table 4.4 Comparing the results of simulation with that of experiment.

Taking away OTF from the cavity, this structure of simulation is the same as the experiment of subsection 3.3. Without OTF, the waveform of the output pulse train is shown in figure 4.14. The pulsewidth is about 10.02ps. The resolution of optical

spectrum analyzer in simulation was set 0.01nm. Figure 4.15 shows the optical spectrum of the simulation result and the right one is the experimental result of 10GHz AML-EFRL in subsection 3.3.1. The bandwidth of the simulation result is about 0.398nm and time-bandwidth product is 0.491. As discussed, filter limits the spectral bandwidth of the pulse. The pulsewidth of the laser is relatively limited. Without the limited of optical band pass filter, the bandwidth and pulsewidth became wider and shorter. Table 4.5 compares the results of simulation with the experiment.

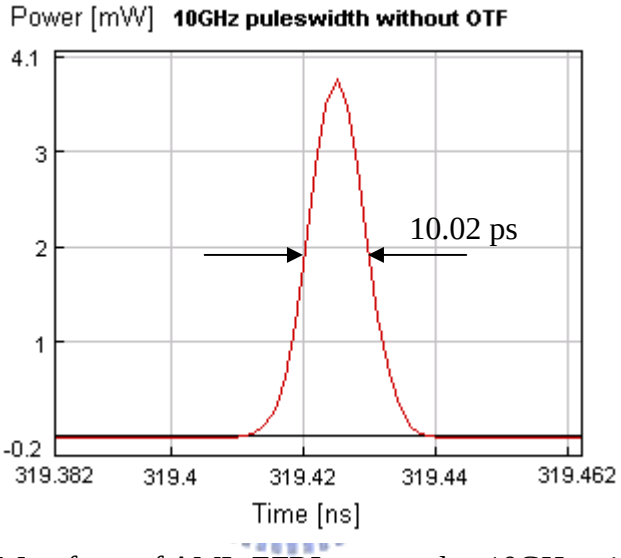

Figure 4.14 Waveform of AML-EFRL operated at 10GHz without OTF.

(FWHM: 10.02ps)

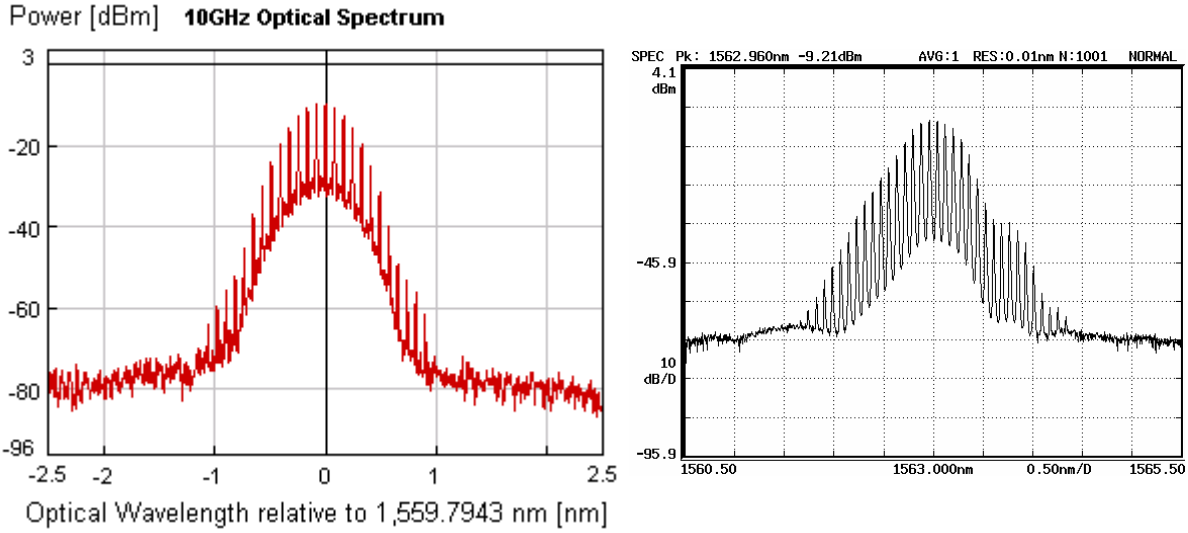

Figure 4.15 Optical spectrum without OTF; the simulation result is shown in the left figure and the right one is the experimental result.

	Simulation	Experiment result w/o filter
Pulsewidth (ps)	10.02	11.07
Bandwidth (nm)	0.398	0.375
Time bandwidth product	0.491	0.510

Table 4.5 Comparing the results of simulation with that of experiment.

4.3.3 Simulation results of 20GHz

The structure of simulations respectively operated at 20GHz and 40GHz are all without "FilterGaussBP", OTF, and the same as the experiment in subsection 3.3.2. Figure 4.16 shows the waveform of the output pulse train. The pulsewidth is measured about 7.75ps. The resolution of optical spectrum analyzer in simulation was set 0.01nm. The vertical and horizontal axis spans were also set the same as the span of optical spectrum analyzer of experimental instrument in reality. The optical spectrum of simulation results is shown as figure 4.17 and the right one is the experimental result of 20GHz AML-EFRL. The bandwidth is about 0.61nm and time-bandwidth product is 0.543. Table 4.6 compares the results of simulation with the experiment.

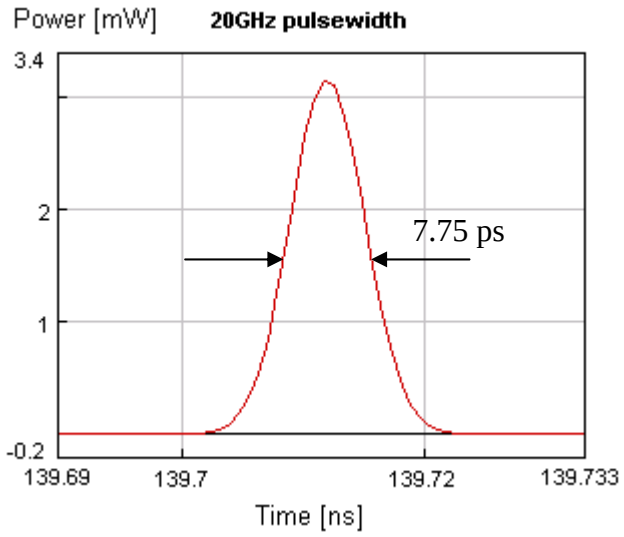

Figure 4.16 Waveform of AML-EFRL operated at 20GHz without OTF.

(FWHM: 7.75ps)

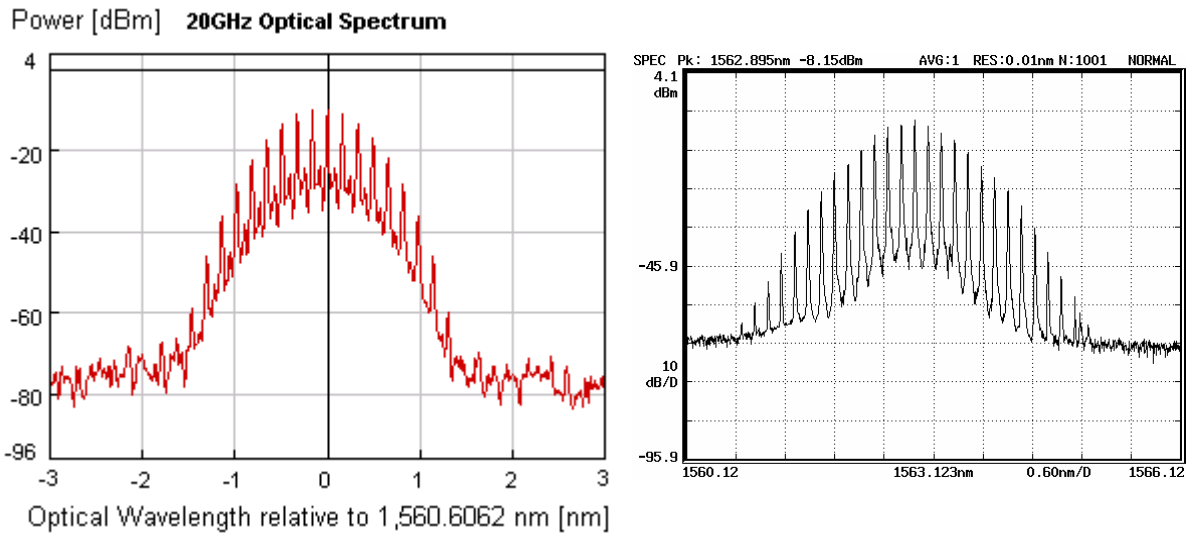

Figure 4.17 Optical spectrum without OTF; the simulation result is shown in the left figure and the right one is the experimental result.

	Simulation	**Experiment result**
Pulsewidth (ps)	7.75	7.81
Bandwidth (nm)	0.61	0.48
Time bandwidth product	0.543	0.461

Table 4.6 Comparing the results of simulation with that of experiment.

4.3.4 Simulation results of 40GHz

Without OTF, the waveform of the output pulse train is shown in figure 4.18. The pulsewidth is about 4.40ps. The resolution of optical spectrum analyzer in simulation was set 0.01nm. Figure 4.19 shows the optical spectrum of the simulation result and the right one is the experimental result of 40GHz AML-EFRL in subsection 3.3.3. The bandwidth is about 1.04 nm and time-bandwidth product is 0.563. Without the limited of optical band pass filter, the bandwidth and pulsewidth became wider and shorter. Moreover, as mentioned in section 2.2.3, the pulsewidth becomes shorter and shorter while the laser is operated at higher repetition rate. Table 4.7 compares the results of simulation with the experiment.

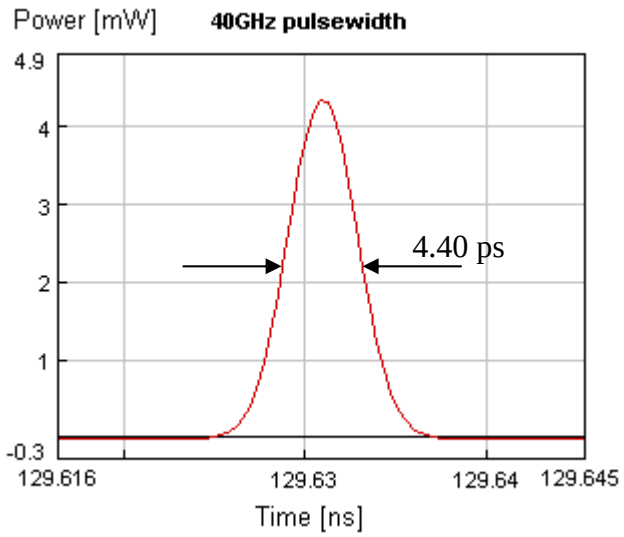

Figure 4.18 Waveform of AML-EFRL operated at 40GHz without OTF. (FWHM: 4.40 ps)

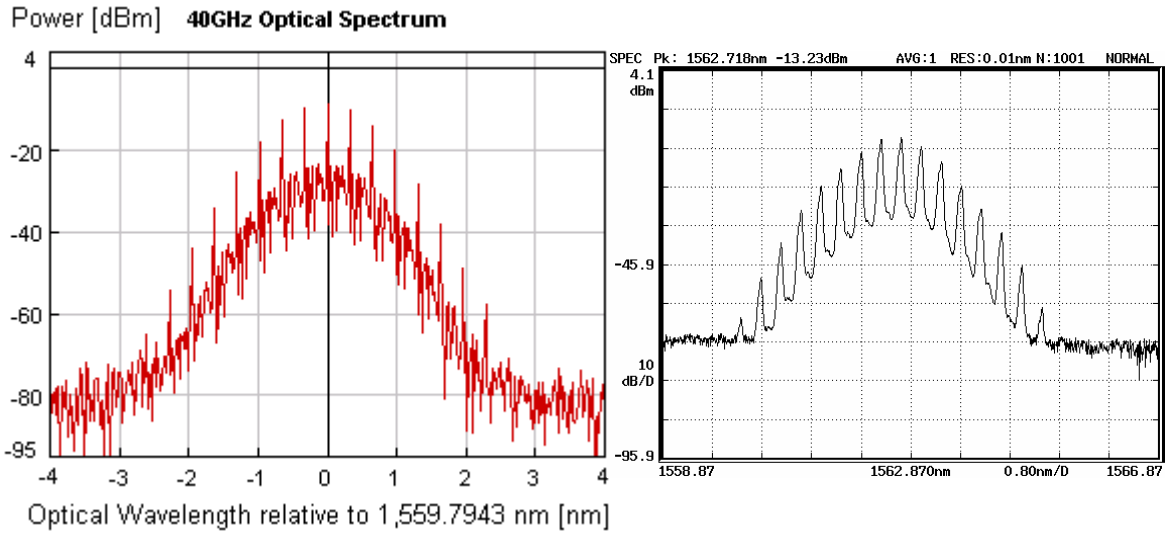

Figure 4.19 Optical Spectrum without OTF; the simulation result is shown in the left figure and the right one is the experimental result.

	Simulation	**Experiment result**
Pulse width (ps)	4.40	3.30
Bandwidth (nm)	1.04	1.20
Time bandwidth product	0.563	0.487

Table 4.7 Comparing the results of simulation with that of experiment.

In simulation results, the values of time-bandwidth product operated at different frequency are all larger than transform-limited, 0.441 for Gaussian shape. Beside, while the operating frequency is increasing, time-bandwidth product becomes larger as listing in the tables. These results are caused by chirp which is induced by cavity dispersion. The group velocity dispersion (GVD) becomes larger and more serious as the laser is operated at higher repetition rate. Actually, the cavity dispersion is not taken into account in transform-limited equation, equation (2.2.10). It can be proven by changing the values of dispersion and dispersion slope of the fiber parameter in simulation. The time-bandwidth product will become close to transform limited while decreasing the values of dispersion and dispersion slope even the laser is operated at 40GHz repetition rate. Actually, changing the values of parameter of "FuncSineB" and "ModulatorMZ" in the simulation are just like adjusting the modulation index in the experiment. It can also change the pulsewidth and bandwidth of the pulse train.

In conclusion, simulation results are all close to experimental results. Thus, the active mode-locked fiber ring lasers can be successfully simulated by using VPI. Besides, by using VPI to simulate, the parameters and characteristic of components can be set and adjusted with far more certainty than in reality. The afraid of mindlessly destroying expensive instrument is unconsidered. It also means that the characteristic of new components which will be put into the experimental structure can be simulated before purchasing. Therefore, the cost can be minimized and the parameters of the components we demand can be confirmed firstly.

CHAPTER 5

Conclusions and Discussions

5.1 Summary of achieved results

A stable optical short pulse source operated at the gigahertz region is strongly required for realizing future ultrahigh-speed optical communication. Many characteristics of mode-locked fiber lasers are much better than semiconductor lasers, such as good pulse quality, transform-limited, and high output power, especially for operating at ultrahigh repetition rate. Besides, among many mode-locking techniques for pulse lasers, active mode-locking is a simple and reliable method for generating stable pulse train in gigahertz regions. Undoubtedly, for application of communication, the active mode-locked erbium-doped fiber laser (AML-EDFL) is a good choice.

There are several special features of AML-EDFL studied in this study. In experimental section, first, the stability of AML-EDFL with a length of signal mode fiber is compensated by polarization controller or not. The pulsewidth of AML-EDFL can be controlled by polarization controller. Second, this study also conducted the differences between AML-EDFL which consists of all polarization-maintaining fiber or not. Third, the pulsewidth and stability of AML-EDFL respectively operated at 2GHz, 10GHz, 20GHz, and 40GHz are compared. In simulation section, the experimental structures are simulated and the results of simulation are compared with the paper and experiment in reality.

Also, in this study, a stable pulse source with high SMSR, high repetition rates, and clean pulse train have been successfully achieved by using AML-EDFL. The AML-EDFL can generate pulse trains with 20GHz repetition rate, clean pulse, and 50dB SMSR. If the AML-EDFL works at 40GHz repetition rate, the pulsewidth is as

short as 3.3ps measured by autocorrelator. Besides, after comparing simulation results with experimental results, the simulations of AML-EDFL have been successfully achieved by using VPI. The new structure can be simulated firstly before experimenting with time and money.

5.2 Future research and Improvement

Future ultrahigh-speed optical communication systems will require stable optical sources which can generate transform-limited pulses at high repetition rates and with low timing jitter. For optical time division multiplexing (OTDM) system, requiring a bit error rate of $< 10^{-12}$, the total timing jitter after the transmission must be <1/14 of the bit slot [33] and is demanded as small as possible. The higher modulating frequency is operated, the more difficult it becomes to maintain the optimum operational condition over a long period. Therefore, how to stabilize the mode-locked laser is one of the most important tasks for recently fiber communication application. There are many kinds of stabilization mechanisms reported, such as regenerative mode-locking [30] and phase locking loop [7] [9]. It has already discussed in section 2.3.

In general, high speed photodetector, amplifier, and high Q filter are needed for most of phase-locked loop (PLL) used to stabilize the mode-locked fiber laser. However, another idea of phase-locked loop of the fiber laser is proposed here. The scheme is shown in figure 5.1. The structure inside the dashed line is the mechanism used for stabilizing AML-EDFL. In theory, a basic PLL consists of phase detector, loop filter, and voltage control oscillator (VCO). The cavity length is controlled by PZT on which part of cavity fiber is wound. Therefore, PZT works as VCO. The clock recovery works as high speed photodetector, amplify, and high Q filter. A fraction of the laser output is received by clock recovery. Then, a sinusoid electrical signal with

synchronous frequency and phase to the laser output will be sent out by clock recovery. The double balance mixer (DBM) works as a phase detector which compares the phase of the sinusoid signal from clock recovery and that of the synthesizer. If a slight change in the cavity length due to temperature variation or mechanical vibrations affects the laser, the error signal immediately occurs from the mixer. After properly processing by low pass circuit, this feedback error signal will automatically control the PZT to compensate the vibrations, which are caused environment perturbations, of the laser cavity length. Then locking occurs.

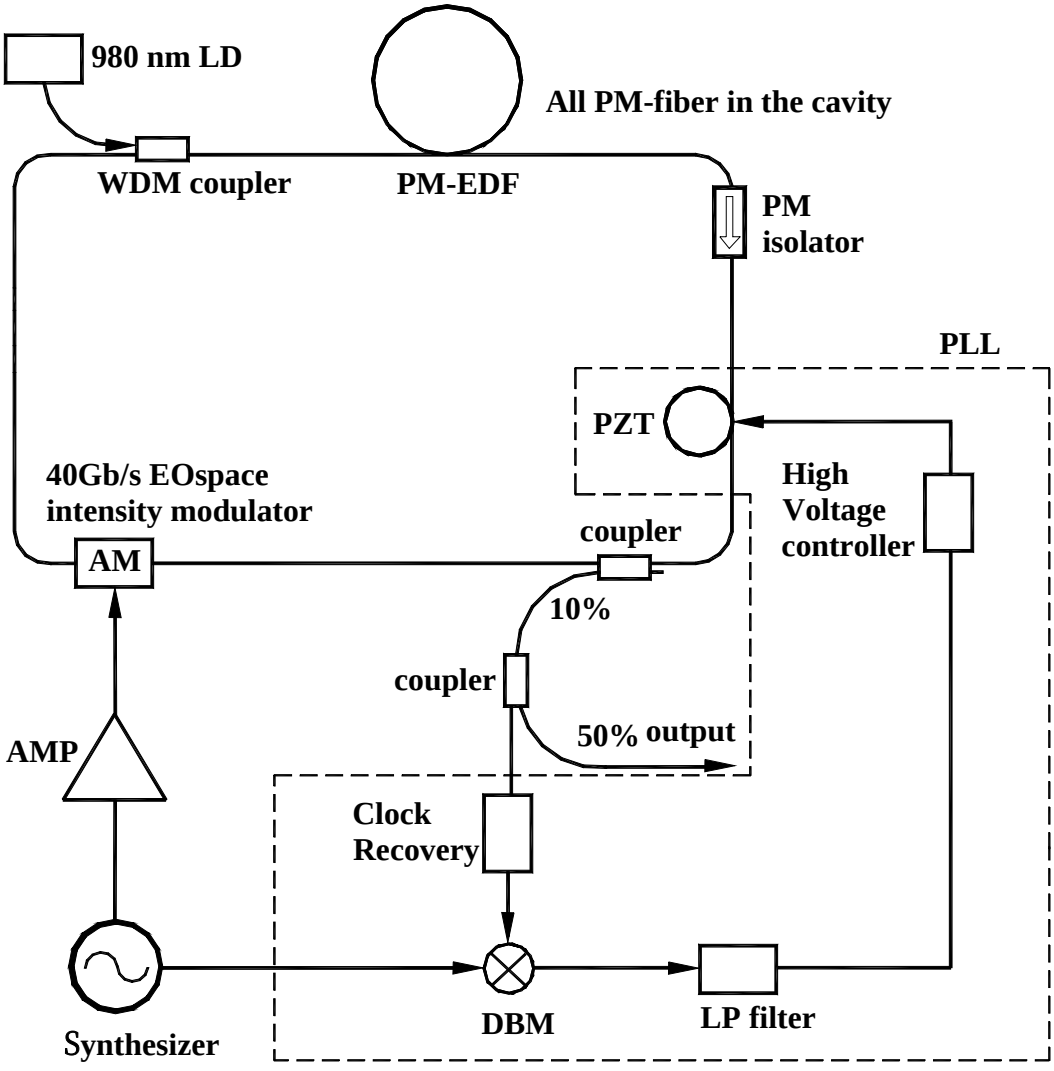

Figure 5.1 AML-EDFL and scheme used for stabilizing it (dashed line); where "DBM" is double balance mixer and "LP filter" is low pass circuit.

The environmentally stable laser also possesses the significant advantage of being driven by synthesizer, allowing it to be synchronized with other components of a communications network.

Moreover, there are some other methods to improve this AML-EDFL. First, the center wavelength of the AML-EDFL can become tunable by placing a wider bandwidth of optical tunable filter in the cavity. Second, a generation of femtosecond pulses in the gigahertz region becomes more and more important in terms of realizing terabit/second communication. As the simulation results, the drawback of active mode-locking, wider pulsewidth can be overcome by placing a length of dispersion shift fiber (DSF) in the cavity. With dispersion management, the balance of self phase modulation (SPM) and group velocity dispersion (GVD) can shorten the wider pulsewidth of active mode-locked fiber laser. Third, the polarization beam splitter (PBS) can be put into laser cavity since it can ensure that the state of the polarization in the cavity aligns to the slow axis of PM fiber. In this way, it is able to build a the powerful active mode-locked erbium-doped fiber laser (AML-EDFL) with stable (low amplitude jitter), high repetition rate, widely tunable wavelength, transform limited, low timing jitter, short pulsewidth, and high extinction ratio pulse train for application of ultra-high speed fiber optical communication.

References

[1] E. Snitzer, “Optical maser action of Nd in a barium crown glass”, *Physical review letters*, 7, 1961, pp.444

[2] J. Stone and C. A. Burrus, *Appl. Phys. Lett.* 23, 388 (1973).

[3] P. C. Becker, N. A. Olsson, J. R. Simpson, “Erbium-Doped Fiber Amplifiers-Fundamentals and Technology”, ACADEMIC PRESS, 1997, pp. 162-163

[4] W. L. Barnes, S.B. Poole, J. E. Townsend, L. Reekie, D. J. Taylor, and D. N. Payne, “Er-Yb and Er doped fiber lasers”, *J. Lightwave Technol*. 1989, 7, pp. 1461

[5] J. D. Kafka, T. Baer, and D. W. Hall, “Mode-locked erbium-doped fiber laser with soliton pulse shaping”, *Opt. Lett.*, 1989, 14, pp. 1269

[6] H. Takara, S. Kawanishi, M. Saruwatari, and K. Noguchi, “Generation of highly stable 20 GHz transform-limited optical pulses from actively mode-locked Er^{3+}-doped fibre lasers with an all-polarisation maintaining ring cavity”, *Electron. Lett.,* 1992, 28, pp. 2095

[7] X. Shan, D. Cleland, and A. Ellis, “Stabilising Er fiber soliton laser with pulse phase locking”, *Electron. Lerr.,* 1992, pp.182

[8] T. Peiffer and G.. Veith, “ 20 GHz pulse generation using a widely tunable all-polarisation preserving erbium fibre ring laser”, *Electron. Lett.* , 1993, pp. 1849

[9] Eiji Yoshida, Naofumi Shimizu, and Masataka Nakazawa, “A 40-GHz 0.9-ps regeneratively mode-locked fiber laser with a tuning range of 1530-1560 nm”, *IEEE Photonics Technology Letters,* 1999, 11, pp. 1587

[10] M. Nakazawa, “ Solitons for breaking barriers to terabit/second WDM and

OTDM transmission in the next millennium", *IEEE J. on selected topics in Quant. Electron.*, 2000 , pp. 1332

[11] L. F. Mollenauer and R. H. Stolen, " The soliton laser", *Opt. Lett*., 1984, pp.13

[12] K. J. Blow and D. P. Nelson, " Improved mode locking of an F-center laser with nonlinear nonsoliton external cavity", *Opt. Lett*., 1988, pp.1026

[13] V. J. Matsas, T. P. Newson, D. J. Richardson, and D. N. Payne, "Selfstarting passively mode-locked fibre ring soliton laser exploiting nonlinear polarisation rotation", *Electron. Lett.*, 1992, pp.1391

[14] K. Tamura, H. A. Haus, and E. P. Ippen, " Self-starting additive pulse mode-locked erbium fibre ring laser", *Electron. Lett.*, 1992, pp.2226

[15] K. Tamura, L. E. Nelson, H. A Haus, and E. P. Ippen, " Soliton versus nonsoliton operation of fiber ring lasers", *Appl. Phys. Lett.*, 1994, pp. 149

[16] P. P Vasil'ev., V. N Morozov., G. T. Pak, Y. U. Popov, M. Yu, and A. B. Sergeev, "Measurement of the frequency shift of a picosecond pulse from a mode-locked injection laser" *Sov. J. Quant. Electron.*, 1985, PP.859

[17] C. J. Chen, P. K. A. Wai, and C. R. Menyuk, *Opt. Lett.*, 1994, pp.198

[18] C. S. Tsai, "Study of an active harmonic mode-locked fiber laser stabilized by a semiconductor optical amplitude", Institute of Electro-Optical engineering in NCTU, master thesis, 2003

[19] Govind P. Agrawal, "Applications of Nonlinear Fiber Optics", Academic Press, Chap. 5, 2001.

[20] R.L. Fork, B. I. Greene, and C.V. Shank, "Generation of optical pulse short than 0.1 psec by colliding pulse mode locking", *Appl. Phys. Lett.*,1981, pp. 671

[21] H. A. Haus, J. G. Fujimoto, and E. P. Eppen, "Structure for additive pulse mode locking", *J. Opt. Soc. Am. B.*, 1991, pp. 2068

[22] K. Tamura, E. P. Ippen, H. A. Haus, and L. E. Nelson, "77-fs pulse generation

form a stretched-pulse mode-locked all-fiber ring laser", *Opt. Lett.*, 1993, pp.1080

[23] S. Y. Chen and J. Wang, "Self-starting issues of passive self-focusing mode locking", *Opt. Lett.*, 1991, pp.1689

[24] Herman A. Haus, "Mode-locking of Lasers", *IEEE J.on Selected topics in Quant. Electron.*, 2000, pp. 1173

[25] M. P. Tian, "High repetition rate femtosecond hybrid mode-locked Er-fiber lasers by asynchronous modulation", Institute of Electro-Optical engineering in NCTU, master thesis, 2003

[26] D. J. Kuizenga, and A. E. Siegman,"FM and AM mode locking of the homogeneous laser-PartI:Theory ", *IEEE K. Quant. Electron*., 1970, QE-6,(11), pp. 694-708

[27] S.G. Edirishinghe, and A.S. Siddiqui, "Stabilised 10GHz rationally mode-locked erbium fibre laser and its use in a 40Gbit/s RZ data transmission system over 240km of standard fibre" *IEE Proc.-Optoelectron*., 2000, pp. 401-406

[28] Z. Ahmed, and N. Onodera, "High repetition rate optical pulse generation by frequency multiplication in actively mode-locked fibre ring lasers", *Electron. Lett.*, 1996, pp. 55-57

[29] R. Kiyan, O. Deparis, O. Pottiez, P. Megret, and M. Blondel, "Long term stable operation of a rational harmonic actively mode locked Er doped fiber laser with repetition rate doubling" *Proc. of European Conf. on Optical Communication*, ECOC'93, September 1999, Nice, France, pp. 180-181

[30] M. Nakazawa, E. Yoshida and Y. Kimura, "Ultrastable harmonically and regeneratively modelocked polarization-maintaining erbium fiber ring laser", *Electron. Lett.*, 1994, pp. 1603

[31] Ivan P. Kaminow and Tingye Li, "Optical fiber telecommunications

IVB –System and Impairments" ACADEMIC PRESS, 2002, Ch 12

[32] VPIphotonics, "Photonic Modules Reference Manual", 2003

[33] Jinno, M., "Effects of crosstalk and timing jitter on all-optical time-division multiplexing using a nonlinear fiber Sagnac interferometer switch", *IEEE J. Quantum Electron. Lett.*, 1994, pp. 2842